Counter-aliasing is better than De-aliasing

Application to Doppler Weather Radar with Aperiodic Pulse Train

Dash, Tworit; Driessen, Hans; Krasnov, Oleg; Yarovoy, Alexander

DOI
10.1109/TGRS.2024.3438567

Publication date
2024

Document Version
Final published version

Published in
IEEE Transactions on Geoscience and Remote Sensing

Counter-Aliasing Is Better Than De-Aliasing: Application to Doppler Weather Radar With Aperiodic Pulse Train

Tworit Dash, *Graduate Student Member, IEEE*, Hans Driessen, O. A. Krasnov, and Alexander Yarovoy, *Fellow, IEEE*

***Abstract*— The challenge of avoiding aliasing in the Doppler spectrum for precipitation is addressed. A novel integrative signal processing approach has been proposed to address the research gaps from various disciplines. The proposed approach consists of several steps. First, an aperiodic way of sampling the echoes (aperiodic sampling refers to aperiodic pulse train in the context of radar echoes in slow time) has been proposed by which the maximum unambiguous Doppler frequency (velocity) is enhanced. Second, the Doppler spectrum moment estimation is performed with the help of a parametric form of its covariance. The performance of the moment estimation is assessed by the bias and the variance in the estimated counterparts. The theoretical variance for the parameter estimation is also derived. An aperiodic pulse train design recommendation has been proposed for adequately and unambiguously estimating the Doppler moments for one extended target (like precipitation). Finally, a spectrum reconstruction technique is implemented after the moment estimation on simulated radar echo samples for a realistic precipitation-like event. The comparison with the other approaches proves its superiority for parameter estimation and Doppler spectrum reconstruction.**

***Index Terms*— Aperiodic sampling, Doppler counter-aliasing, Gaussian processes (GP), hyperparameter estimation, radar signal processing.**

I. Introduction

IN THE field of weather monitoring, the ability to accurately estimate the Doppler velocities of precipitation plays a pivotal role in the safety and operations across various sectors, including aviation.

Although modern X-band weather radar sensors have been instrumental in estimating properties related to precipitation, some challenges remain in the realm of Doppler radial velocity/frequency spectrum estimation. One such challenge is the aliasing of the Doppler spectrum. Aliasing is caused by the sensor configuration, which limits the reconstructed velocities/frequencies to the Nyquist unambiguous velocity/frequency limit. Aliasing causes ambiguity when the targets of interest move with higher velocities than this limit.

Manuscript received 22 March 2024; revised 2 July 2024 and 31 July 2024; accepted 1 August 2024. Date of publication 5 August 2024; date of current version 21 August 2024. This work was supported by the European Regional Development Fund (ERDF) via the Kansen voor West II Program under the Project "Airport Technology Lab." *(Corresponding author: Tworit Dash.)*

The authors are with the Microwave Sensing, Signals and Systems (MS3), Delft University of Technology, 2628 CD Delft, The Netherlands (e-mail: T.K.Dash@tudelft.nl; J.N.Driessen@tudelft.nl; O.A.Krasnov@tudelft.nl; A.Yarovoy@tudelft.nl).

Digital Object Identifier 10.1109/TGRS.2024.3438567

Doppler spectrum aliasing is not a new problem. It can also be found in other radar-related applications, such as automotive and millimeter wave applications [1], [2], [3], and synthetic aperture radar (SAR) remote sensing [4], [5], [6]. Doppler aliasing is also observed in studies other than radar, such as in ultrasound and ultrasonography sensing [7], [8], [9]. However, this article focuses on the impact of aliasing on parameter retrievals and Doppler spectrum reconstruction for precipitation only. Before discussing how aliasing affects the parameters related to the Doppler spectrum, let us discuss which parameters are typically retrieved from the precipitation Doppler spectrum.

The most popular retrieval practice is to store only the first three statistical Doppler moments [10], [11], [12], [13], [14], [15], [16], [17]. The zeroth moment is the total power received from the radar echoes, and it is a measure of the intensity of the precipitation. The first Doppler moment is often related to the mean radial velocity of the raindrops. The square root of the second moment around the mean Doppler velocity (second central moment) is a measure of several statistical effects, such as turbulence in the rain and the effect of the antenna beam shape [11], [18], [19], [20], [21], [22].

The parameter that is heavily affected by aliasing is the mean Doppler velocity. It is further used to compute the vertical raindrop speed (also known as the terminal fall velocity) and the horizontal wind field as a function of space and time [23], [24], [25], [26], [27], [28], [29]. Some de-aliasing techniques are addressed in the post-processing phase to correctly locate the mean Doppler velocity by using information from other sources (also sometimes non-radar sources). These methods detect sharp mean Doppler velocity transitions across resolution volumes, assuming smooth and homogeneous wind fields. In these post-processing de-aliasing algorithms, challenges include missing or corrupted mean Doppler velocity retrievals, addressed by advanced tools like [30] and [31, Ch. 5] (model-based optimization technique). Some techniques incorporate temporal reflectivity and mean Doppler velocity variability to relax the assumption of a homogeneous wind field [32], albeit at increased computational cost. In addition, these temporal approaches may still rely on assumptions like reflectivity conservation [33] (often associated with fluid flow).

Aliasing in many existing sensor systems is inevitable due to one crucial system design related to the transmitted

radar pulse train: the fixed interval between two successive transmitted signals [also known as the pulse repetition time (PRT)]. This type of signal sampling is known as periodic sampling. Therefore, the apparent strategy that has been tried to avoid aliasing is an aperiodic way of sampling the signal. Despite numerous efforts to realize optimized sampling strategies and parameter estimation techniques, aliasing remains an issue due to the lack of an appropriate frequency-domain conversion technique (leading to much higher ambiguous lobe levels). One such sampling strategy is the staggered sampling sequence, where the sequence alternates between two periodically sampled sequences [34], [35]. Although the de-aliasing scheme presented with staggered sequences is computationally efficient, they are susceptible to errors introduced by the individual velocity estimates of the constituent sampling sequences. External inputs like spatial and temporal continuity of Doppler moments are often used to mitigate such errors [34], [36].

To adequately address aliasing issues, one needs to broaden the research horizon, investigate the problem of ambiguity from various perspectives, and combine the outcomes of these investigations in one generic approach.

In this article, we try to construct a generic, novel, and integrative approach that exploits an aperiodic sampling sequence. By an integrative approach, we mean that complementary knowledge from different research areas has been brought together to address the problem of ambiguity (the word "integrative" is emphasized to show that it is not just a combination of techniques).

The various research areas that contribute to the integrative approach proposed are as follows.

1) The Nyquist limit for aperiodically sampled signals.
2) Radar signal processing approaches to deal with aperiodically sampled signals in the frequency domain.
3) Frequency-domain conversion techniques specifically designed for aperiodic sequences.
4) Model-based parameter estimation and reconstruction of Doppler frequency spectrum.

Each topic mentioned above in the literature considers several aspects of aliasing but ignores certain others. Hence, the significant contribution of this article is a novel integrative approach for radar-based weather monitoring that addresses the research gaps among all the areas mentioned above.

The proposed approach is based on complex Gaussian process (CGP) regression on aperiodically sampled signals. It is a parametric technique where parameter estimation is performed first, followed by spectrum estimation. Apart from the novel integrative approach to address the gaps and the advantages of each research area, we present an intuitive study of the Doppler parameter estimation performance analysis using the proposed technique. This study presents the benefits of the integrative approach and shows the physical limiting conditions for accurately estimating Doppler velocity/frequency parameters unambiguously. The parameter estimation is compared with the state-of-the-art Doppler moment estimators, such as the discrete Fourier transform (DFT), pulse pair (PP), the parametric spectrum estimator (PSE) [11], and a staggered sampling approach [34]. The performance of the parameter estimation is also studied with respect to the nonlinearity in the sampling sequence. Furthermore, the Doppler spectrum is reconstructed in the frequency domain directly using the CGP posterior [12] and compared with the nonuniform DFT-based periodogram (nonuniform Schuster periodogram). The integrative approach proposed in this article is classified as a counter-aliasing technique (and not a de-aliasing technique), where the Doppler velocities and the spectrum are estimated directly from an aperiodically sampled sequence. It does not involve any de-aliasing scheme where true velocities are estimated based on some pre-estimated velocities (e.g., staggered sampling) or extra information (e.g., Unfold Radar Velocity algorithm or UNRAVEL [30]).

The main body of this article is structured as follows. Section II presents a broad overview of the state of the art and the rationale behind the proposed approach. Section III explains the signal and the covariance model for typical precipitation events. Section IV is devoted to estimating hyperparameters in the CGP covariance model (parameters of the Doppler spectrum). Section V presents the technique for directly reconstructing the Doppler spectrum in the frequency domain using time-domain measurements. Section VI presents hyperparameter estimation performance analysis results and Doppler spectrum reconstruction with simulated radar echoes. Finally, Section VII concludes this article.

II. State of the Art and the Rationale Behind the Proposed Approach

In this section, we present a comprehensive analysis of all the fields of study introduced in Section I to understand better the issue of aliasing from different perspectives. We present the missing analysis and research gaps in all these areas of study. Finally, we show the rationale behind the proposed integrative approach and its operation.

A. Nyquist Limit for Aperiodically Sampled Signals

For any frequency-domain interpretation, it is essential to define the maximum observable frequency allowed (also called the Nyquist limit) based on the measurement setup. The Nyquist frequency limit is the maximum frequency observable as a result of digitally sampling a signal. The Nyquist limit is very well defined when the signal is sampled periodically ($f_{\mathrm{NY,per}} = 1/(2\Delta t_{k,\mathrm{per}})$), where $\Delta t_{k,\mathrm{per}}$ is the periodic sampling interval. However, the Nyquist limit for aperiodically sampled sequences is very ill-defined in the literature. A definition is given in [37] for any sampling sequence (note the $\leq$)

$$f_{\mathrm{NY}} \leq \frac{1}{2} 10^{D} \text{ Hz} \tag{1}$$

where D is the decimal point precision. For example, if we consider a time sequence where we can measure time with six decimal point precision, the maximum Nyquist limit can be as large as 0.5 MHz if the sequence is aperiodic in nature. This property of breaking the periodicity of the sampling sequence is beneficial in avoiding ambiguity or aliasing. The corresponding velocity parameters are related to the frequency as $v = f\lambda/2$, where λ is the radar central wavelength.

Therefore, the maximum unambiguous velocity of any sampling sequence as V_a is given by

$$V_a \leq \frac{\lambda}{4} 10^D \text{Hz}. \tag{2}$$

Throughout this article, we use the subscript "per" for periodic sequences, "ap" for aperiodic sequences, and "st" for staggered sequences for clarity.

A similar conclusion can be drawn from the literature describing staggered sampling sequences. A staggered sampling sequence is a sampling sequence that switches among several periodic sampling sequences. In [34] and [35], the staggered sequence is made with two periodic sampling sequences whose ratio of sampling intervals is denoted as m/n, where m and n are integers. If the sampling intervals are $\Delta t_{\text{st},1}$ and $\Delta t_{\text{st},2}$, the underlying sampling interval that satisfies both should be the greatest common divisor of $\Delta t_{\text{st},1}$ and $\Delta t_{\text{st},2}$. If this underlying sampling interval is denoted as Δt_u, the intervals $\Delta t_{\text{st},1}$ and $\Delta t_{\text{st},2}$ are integer multiples of Δt_u ($\Delta t_{\text{st},1} = m\Delta t_u$, $\Delta t_{\text{st},2} = n\Delta t_u$). This underlying sampling sequence decides the Nyquist frequency of the staggered sequence, i.e., $f_{\text{NY,st}} = 1/(2\Delta t_u)$Hz. If m and n are relatively prime, the largest time interval of which $\Delta t_{\text{st},1}$ and $\Delta t_{\text{st},2}$ are integer multiples is 10^{-D} s. The Nyqyuist frequency in this case is $f_{\text{NY,st}} = 1/2 \times 10^D$Hz. Therefore, the expression in (1) is justified for any sampling sequence. To sum up, in any aperiodic sequence in which there is no obvious greatest common divisor for all sampling intervals in the sequence, one can safely consider that there is still an underlying periodic structure (grid) of which all the sampling intervals are integer multiples. It is $\Delta t_u = 10^{-D}$s.

Several methods exist to create an aperiodic sampling sequence, such as linearly increasing chirp sampling, random sampling based on a Gaussian distribution, and sinusoidal sampling [38], [39], [40]. However, choosing one for the required application of interest can be challenging. In this article, we restrict ourselves to using only the log-periodic sampling sequence and compare it with the conventional periodic and staggered sampling cases. First, we choose log-periodic sampling because it is inherently irrational, and the user can define the precision based on the desired decimal point accuracy [an equality sign can be realized for this sampling in (1) and (2)]. The requirement for a certain number of decimal point accuracy can arise from hardware constraints for measuring the sample instances. Second, the parameters of the sampling rule can be tuned to ensure the minimum sampling interval does not exceed a threshold; hence, it allows for a fair comparison with a corresponding periodic sampling sequence. Third, its performance in the case of point frequency response has been studied, and it is the best among all the other nonuniform sampling strategies in terms of sidelobe levels [38]. A detailed explanation of the sampling rule with the log-periodic sampling strategy has been presented in Section VI.

The application of log-periodic sampling can be found in the field of antenna array design [41] (here, the sampling refers to the physical placement of antennas in space) and Doppler processing [38]. In these studies, the effect of the log-periodic sampling is studied in the case where the signal consists of one sinusoid in the presence of white Gaussian noise. However, these analyses do not study the performance when the frequency spectrum of the target response is continuous and extended, like a typical precipitation-like Doppler spectrum.

B. Radar Signal Processing Approaches to Deal With Aperiodically Sampled Signals in the Frequency Domain

As the raw radar echoes are collected in the physical time domain, extra processing is often applied to visualize it in the frequency domain. Let us consider the unambiguous velocity interval being $[-V_{a,\text{per}}, V_{a,\text{per}}]$ for a traditional periodic sampling case.

Let us assume that the majority of the scatterers (raindrops, in our case, in one big radar volume) are moving with an average velocity of $v = 1.5\ V_{a,\text{per}}$ in reality. We construct the Doppler power spectrum with a traditional frequency-domain technique; we will find that the majority of the scatterers are moving with $(-V_{a,\text{per}} + 0.5 \times V_{a,\text{per}})$, meaning that the excess from $V_{a,\text{per}}$ is circularly shifted and added in the opposite direction (at $-V_{a,\text{per}}$). If we construct the power spectrum for velocities $[-pV_{a,\text{per}}, pV_{a,\text{per}}]$, $p > 1, p \in \mathbb{Z}^+$ in the hope of finding the true mean velocity at $1.5 \times V_{a,\text{per}}$ with the maximum power level, to our surprise, we will find that the power levels of all radial velocities that are of the form $v \pm 2pV_{a,\text{per}}$ are the same; causing ambiguity (these lobes in the frequency domain are called as "grating lobes" or "ambiguous lobes"). As discussed in Section II-A, in principle, with a proper frequency-domain conversion technique, an aperiodic sequence should decrease these higher ambiguous lobe levels, making it unambiguous.

However, there are three missing pieces in the radar literature related to this issue. First, a suitable frequency-domain conversion technique is unavailable to realize an unambiguous frequency spectrum for aperiodically sampled signals. Many studies use a DFT-based periodogram approach (Schuster periodogram [42]) to construct the frequency spectrum for aperiodically sampled signals.

However, using a simple DFT on aperiodically sampled signals is inefficient as the DFT approach inherently constructs the resonant peaks based on the sampling intervals. If the sampling interval is aperiodic, the DFT response becomes noise-like. Although the ambiguous lobe levels can be reduced, they are not considerably suppressed. These partly suppressed ambiguous lobes that create noisy artifacts in the spectrum will be referred to as "ambiguous artifacts" further in the text. The term "ambiguous locations" refers to the locations in frequency where ambiguous lobes are expected. For example, aperiodic sampling has been used for Doppler frequency response for time series [38]. However, the analysis is restricted to point targets, and the frequency response is studied only with the Schuster periodogram, resulting in higher levels of ambiguous artifacts. Another example can be found in spatial aperiodic sampling, which is deliberately used in antenna array design for communication and radar applications for two main purposes. The first purpose is to increase the

aperture size with fewer antenna elements than if designed periodically to have a larger gain and suppression of the ambiguous lobes to avoid confusion regarding the angle of arrival (radiation pattern). However, the radiation patterns of these antenna arrays in these studies are usually computed with a Schuster periodogram, resulting in higher levels in the ambiguous artifacts. Some extra processing is usually applied to suppress the artifacts further [43], [44].

Second, the Nyquist limit of such aperiodic sampling strategies is not well discussed. Third, the effect of aliasing on continuous and extended frequency responses (like that from precipitation-like Doppler spectrum) is not discussed. For continuous and extended frequency response, by the application of the Schuster periodogram, ambiguity remains a problem when the normalized spectral width of the target crosses a threshold, even with an aperiodically sampled sequence. It is demonstrated in Section VI. Usage of Schuster periodogram can be found in [45] for log-periodic sampling for weather Doppler radar data. As this periodogram produced higher levels of ambiguous artifacts (especially deteriorating the frequency response as the spectral width increases), it suggests the use of techniques like the iterative adaptive approach (IAA) proposed in [46] to suppress the artifacts further. The frequency grid chosen for this analysis can be very large; therefore, the computational complexity grows as a function of the number of iterations in the IAA algorithm. If used incorrectly, the useful spectra levels can also get suppressed along with the artifacts. Therefore, special care must be taken when applying these techniques.

A useful de-aliasing algorithm has been presented for the mean Doppler frequency in the study of the staggered sampling sequence of [34]. However, the algorithm is highly sensitive to errors in the individual estimates of the mean Doppler frequency by the two constituent periodic sampling sequences. Statistical performance analysis of the estimate of the mean Doppler frequency is not presented with respect to the spectral width in [34]. Therefore, Section VI of this article presents the performance of the Doppler moments estimation with a staggered sampling sequence with a staggered sampling ratio $m/n \approx 2/3$ and is compared with the proposed log-periodic sampling sequence.

C. Frequency-Domain Conversion Techniques Specifically Designed for Aperiodic Sampled Signals

After discussing the problem in the radar domain, we extend the analysis to the spectral estimation domain. Therefore, we explore the literature based on spectrum estimation explicitly theorized for aperiodically sampled signals [47], [48], [49]. These techniques are typically found in the radio astronomy literature, where the received signal is usually not acquired at periodic intervals.

The Lomb–Scargle periodogram mentioned in [47], [48], and [49] is based on a least-squares fit of the observations with a Fourier-like basis, having discrete frequencies, but different amplitudes for the real and imaginary parts. The study drawn from a Bayesian periodogram analyzed by Jaynes and Bretthorst [50] shows that the Lomb–Scargle periodogram is the optimal periodogram for aperiodic sequences, assuming that the signal is resonant with one sinusoid in the presence of white Gaussian noise. The Bayesian formalism of the generalized Lomb-Scargle periodogram is given in [48] and [51].

The exponentiation of the generalized Lomb–Scagrle periodogram for sinusoids with white Gaussian noise, as explained in [48], acts like a spectral window, where the idea is to suppress the sidelobes and ambiguous artifacts significantly while retaining the shape of the main lobe; however, exponentiation should be performed carefully [37].

Although the nuances of such approaches are discussed, derivation of the power spectrum with a generalized Lomb–Scargle periodogram [52] for a complex signal (with real and imaginary parts of the signal acquired at the same instant with no decay factor in the model, demonstrates no difference from the classical Schuster periodogram. On the other hand, there is also a minimal difference in the sidelobe levels, even for real-valued signals. These techniques are also often designed for a Dirac comb-like frequency response (a combination of pointed frequencies placed at sparse locations in the frequency domain). The issues related to extended frequency responses still remain.

The staggered sampling of [34] is used in [35] to construct the autocorrelation spectral density (ASD). This technique is useful in separating clutter from precipitation. Although it shows the ASD preserves the spectral response of the clutter near the zero frequency and the sidelobe levels are adequate enough in the frequency range $f < f_{\mathrm{NY}}/5$ for a staggered sampling ratio of $m/n = 2/3$, it does not show the power levels at the ambiguous locations. Therefore, it is difficult to judge the ambiguous artifacts in the construction of ASD.

The approach proposed in this article is compared with the aperiodic Schuster periodogram in Section VI, because the radar echoes in slow time are also complex-valued, and the real and imaginary parts of the signal are received at the same time instant.

D. Model-Based Parameter Estimation and Reconstruction of Doppler Frequency Spectrum

Using model-based techniques, some crucial parameters of the Doppler spectrum can be estimated first before reconstructing the spectrum. The literature on Gaussian processes (GP) addresses this issue. The covariance of the signal is modeled with these parameters. These parameters of the GP are estimated by performing the maximum likelihood estimation (MLE) on the marginal log-likelihood.

There are a few missing points in all these studies. The literature that studies the signal reconstruction in its original domain (e.g., in this case, the time domain) often ignores the rebuilding of the frequency domain [53]. The literature that deepens into the frequency-domain reconstruction often avoids the aliasing issue and complex signals and only deals with real-valued signals [54]. The ones that study complex signals with CGPs and frequency-domain reconstruction [12] do not address the ambiguity issues in detail. In all the GP literature, the spectrum/signal reconstruction is often assumed to be nonparametric. Still, in reality, the covariance of the signal is

modeled with some parameters. These parameters are known as hyperparameters, and the signal/spectrum reconstruction is highly dependent on the estimated counterparts of these parameters.

The periodic covariance models (or periodic kernel functions) of the GP literature often have a quantity that can characterize an extended object (the spectral width explained earlier in Section I) and a quantity that characterizes the target's location (the mean Doppler frequency explained earlier).

For correlating the meaning of these parameters with normalized weather Doppler parameters mentioned in Section I, it is advised to check the literature: γ_q, and θ_q of [54, eq. (15)] is similar as $2\pi^2\sigma_{fn}^2$, and μ_{fn} of [12, eq. (23)], respectively.

However, as these studies focus on reconstructing the signal, they often do not present a performance analysis of the estimation of the hyperparameters. For example, the focus of [55] is finding a global maximum in the log-likelihood containing these parameters. It is understood that they try to find the global maxima in an attempt to reach the true location of the target(s) by avoiding getting stuck at the ambiguous lobes (the local maxima). However, the performance of such hyperparameter estimations has not been appropriately studied for extended targets (by varying the normalized spectral width).

It is also plausible that for certain values of normalized spectral widths, the global maxima for the location parameter (mean Doppler) becomes highly sensitive to the measurements, and the solution becomes truly ambiguous.

These techniques are also often applied to signals with missing observations, but they do not often study the aliasing phenomenon.

For the application discussed in this article, the hyperparameters directly relate to physical phenomena in the atmosphere and are highly important for wind and turbulence predictions. As described in [10] and [11], modern fast-scanning weather radars do not have enough time on the extended target volumes due to their fast scanning nature. The "CGP" approach is often preferred, especially when the number of data points is small. Therefore, this article presents an estimation of these parameters with a few data points mimicking fast scanning radars.

E. Rationale Behind the Proposed Approach

In this section, we present the proposed integrative approach for counter-aliasing. A log-periodic sampling is adopted for this study as it has a good frequency response for point-like targets [38]. The explanation is given in Section II-A.

After that, we formulate the signal as a CGP with a covariance function that combines components containing three parameters (their strength, location, and width).

In this article, hyperparameter estimation is conducted to assess the applicability of the proposed log-periodic sampling, focusing on the spectral width's impact on the performance. The spectral width, also a hyperparameter, reflects the Doppler power spectrum's "flatness." Larger spectral widths make unambiguous mean Doppler frequency detection more challenging. The study compares hyperparameter estimation performance with classical Doppler moment estimators like DFT-based and PP algorithms and a parametric spectrum estimation approach [11] (referred to as PSE). The novelty lies in examining how parameter estimations are influenced by this spectral width, addressing the question of "How wide is too wide?" The word "wide" is used to dictate a larger spectral width; typical spectrum width values for severe storms are discussed in [56]. Next, this article discusses the physical limitations of accurately estimating parameters. By enhancing the Nyquist unambiguous limit with the chosen sampling strategy, the study avoids global maxima estimation, favoring Newton-based gradient descent optimization from random starting points.

The performance analysis of such estimations is presented in terms of the bias and variance in the estimation (by performing a Monte Carlo simulation). The theoretical variances of such parameter estimation are also derived and compared with the numerical variances obtained from the simulations.

Then, the power spectrum reconstruction is carried out directly in an extended frequency domain (avoiding the reconstruction in the time domain) using CGP posterior to reduce computation complexity [12], [54].

Furthermore, a realistic simulation of weather radar echoes is performed, having three extended targets (one clutter and two extended precipitation-like targets), and the reconstruction is shown using the proposed integrative approach.

III. Signal and Covariance Model

The echo sample model with time is given in [10] and [11]. The signal at each instant of time is an ensemble of the backscattered signals from each scatterer in the radar resolution volume. The signal is assumed to be stationary (meaning that the frequency content remains constant over a short period). The noise in the measurement model is assumed to be zero-mean complex white Gaussian. The measurement model is given as

$$\mathbf{z} = \mathbf{s} + \mathbf{n}, \quad \{n_k\}_{k=0}^{N-1} \overset{i.i.d}{\sim} \mathcal{CN}\left(0, \sigma_n^2\right) \tag{3}$$

where $\mathbf{z} = [z(0), z(1), \cdots, z(N-1)]^T$ is the complex measurement vector with N echo samples, $\mathbf{s}$ is the signal vector, and $\mathbf{n}$ is the noise vector with noise variance σ_n^2. The signal is assumed to be a circularly symmetric CGP (proper CGP) [12]. Proper CGPs have the following properties:

$$\mathbb{E}\left[z(t_a)z(t_b)^*\right] = C(t_a, t_b) = C(t_a - t_b) \tag{4}$$

$$\mathbb{E}[z(t_a)z(t_b)] = 0 \tag{5}$$

where C is the covariance of the echo samples and only a function of the time difference between the echoes ($t_a - t_b$), and the asterisk (*) refers to the complex conjugate. The expression in (5) is the pseudo covariance, 0 for a proper CGP. The pseudo covariance of Doppler weather radar echoes is 0 because the signal model [11, eqs. (3) and (4)] assumes that the initial positions of the scatterers are uniformly distributed in the resolution volume. The covariance is modeled as a mixture of periodic kernels with Gaussian envelopes

$$C(\tau) = \sum_{q=1}^{Q} P_q \exp\left(-2\pi^2\sigma_{q,fn}^2\tau^2\right)\exp\left(j2\pi\mu_{q,fn}\tau\right) \tag{6}$$

where Q is the number of Gaussian components in the mixture model, P_q is the total power, $\mu_{q,fn} = \mu_{q,v}/(2V_{a,\text{per}})$ is the normalized mean Doppler frequency, and $\sigma_{q,fn} = \sigma_{q,v}/(2V_{a,\text{per}})$ is the normalized Doppler spectrum width of the qth component in the mixture. The term j refers to the imaginary unit $(-1)^{1/2}$. The $V_{a,\text{per}}$ is the maximum unambiguous velocity for a periodic sampling case, and the parameters are normalized with $2V_{a,\text{per}}$ to make the performance comparison and analysis easier. For velocity estimates, these normalized quantities can be scaled with $2V_{a,\text{per}}$. The periodic sequence considered here is a sequence having a sampling interval similar to or lesser than the minimum sampling interval of the aperiodic sequence. The details of the sampling sequences that are used in this article for performance analysis are given in Section VI-A.

The motivation for modeling the weather radar signal covariance as a combination of multiple periodic Gaussian kernels is the following.

1) If the radar volume is considerably large and spans multiple altitudes in the atmosphere, there is a chance that the wind field is not constant in the volume and can have different mean velocities in the response.
2) Convective rain and vortices can contain multiple extended components in the Doppler response [57], [58].
3) Due to several types of clutter, an extended target response can be observed at the zero Doppler [59], [60], [61].

The approach developed in this article is also applicable to persistent stratiform rain events. The stratiform rain Doppler spectrum is usually modeled as one Gaussian-shaped continuous and extended spectrum. However, as mentioned earlier, if the radar volume is large and covers several altitudes, it can also contain multiple Gaussian-shaped spectra at different mean Doppler velocity locations (due to inhomogeneity in the wind field as a function of height), and the Q value can be adjusted in that case.

As the proposed approach can also handle a small amount of echo samples, the change in the Doppler velocity parameters can be tracked in time, which is beneficial for applications like hydrology.

In this article, the Doppler covariance is modeled with mean velocity and spectral width. However, applications like hydrology may need more atmospheric parameters like the drop size distribution (DSD) parameters or the DSD-derived parameters such as the rainfall rate and the terminal fall velocity of raindrops. The covariance can also be modeled with these parameters and considered in the future.

The signal z can then be considered a zero-mean proper CGP

$$\mathbf{z} \sim \mathcal{CGP}(\underline{\mathbf{0}}, \mathbf{C_{CN}}, \mathbf{0}) \tag{7}$$

where the first entry is the mean, the second is the covariance, and the third is the pseudo-covariance. The covariance $\mathbf{C_{CN}}$ is nothing but the complex covariance $\mathbf{C}$ with added covariance of the zero-mean complex white Gaussian noise $\mathbf{C_{CN}} = \mathbf{C} + \sigma_n^2 \mathbf{I}_{N\times N}$.

Algorithm 1 Optimization Algorithm

1: **for** $i = 1$ to K **do**
   1) Initialize parameters $\Theta_i^{(0)} \sim \mathcal{U}(\Theta_l, \Theta_u)$
   2) $\hat{\Theta}_i = \max_\Theta \log(p(\mathbf{z}|\Theta))$
   3) $J_i = \log(p(\mathbf{z}|\hat{\Theta}_i))$
2: **end for**
3: $i_{\max} = \max_i J_i$
4: $\hat{\Theta} = \hat{\Theta}_{i_{\max}}$.

IV. Hyperparameter Estimation

The hyperparameters are estimated by maximizing the log-likelihood

$$\log(p(\mathbf{z}|\Theta)) = -\frac{1}{2}\mathbf{z}^H \mathbf{C_{CN}}^{-1}\mathbf{z} - \frac{1}{2}\log(|\mathbf{C_{CN}}|) - \frac{N}{2}\log(2\pi) \tag{8}$$

$$\hat{\Theta} = \max_\Theta \log(p(\mathbf{z}|\Theta)). \tag{9}$$

A constrained quasi-Newton optimization strategy is applied to optimize it. It uses active-set method and the limited memory Broyden–Fletcher–Goldfarb-Shanno (L-BFGS) algorithms [62]. The optimization is performed several times with random starting points (following a uniform distribution) inside the parameter space to avoid getting stuck at local minima if any. The normalized mean Doppler velocity parameter space is chosen as several multiples of the Nyquist interval of the equivalent periodic sequence. The algorithm adopted for optimization is presented in Algorithm 1.

Here, $\Theta_i^{(0)}$ are the starting points of the parameters in iteration i, and Θ_l, Θ_u are the lower and upper limits of the parameter space, and K is the number of iterations. The values of these quantities for our simulation purposes are given in Section VI.

Several other strategies can also be applied for global maxima optimization, such as Markov chain Monte Carlo (MCMC) sampling methods [63]; we avoid using these techniques as they are computationally expensive.

For the hyperparameter estimation performance analysis in Section VI-B, only one of these components ($Q = 1$) is studied to make an intuitive comparison among the different approaches. The total power P, and the noise variance σ_n^2 are considered known quantities for this analysis.

In Section VI-E, three components are considered: two for two extended weather targets and one for clutter ($Q = 3$). In this case, the number of unknown hyperparameters is 8. The mean frequency of the clutter and the noise variance are considered known in this case. The unknown parameters are then the total powers of all the components, the mean frequencies of the extended targets, and the spectral widths of extended targets and clutter. The information on the number of components is assumed to be a known quantity. We do not study closely spaced multiple extended weather targets. If the number of components is unknown, it can also be used as a parameter to be estimated. There are several techniques to address the estimation of Q. It can be separately estimated

using the Akike information criterion (AIC) and the Bayesian information criterion (BIC) [64]. It can also be estimated jointly with the other parameters if a reversible jump MCMC parameter estimation strategy is adopted [65].

For very closely spaced extended targets with velocities modeled with a mixture model, it is a difficult problem and requires many data points. Even with many data points, the parameter estimation is difficult in practice for several other factors and requires dedicated attention [66].

V. Spectrum Reconstruction

After the estimation of the hyperparameters, the Doppler spectrum can be reconstructed by the posterior of the proper CGP. The posterior of a zero-mean proper CGP prior is also a proper CGP. As this is a Bayesian technique, many realizations of the reconstruction can be drawn (sampled) from this posterior distribution. The posterior can be computed both in the time and frequency domain directly [12], [54]. The covariances are rearranged to make them real-valued instead of complex ones. For CGPs, the real-valued covariances can be represented as

$$\mathbf{C}_{\mathrm{R}}=\begin{bmatrix}\mathbf{C}_{\mathrm{rr}} & \mathbf{C}_{\mathrm{ri}}\\ \mathbf{C}_{\mathrm{ir}} & \mathbf{C}_{\mathrm{ii}}\end{bmatrix} \tag{10}$$

where $\mathbf{C}_{\mathrm{rr}}$ is the covariance of the real part with itself, and $\mathbf{C}_{\mathrm{ii}}$ is the covariance of the imaginary part with itself. The entries $\mathbf{C}_{\mathrm{ri}}$ and $\mathbf{C}_{\mathrm{ir}}$ are the covariances between the real and imaginary parts. For a proper complex CGP, $\mathbf{C}_{\mathrm{rr}}=\mathbf{C}_{\mathrm{ii}}$ and $\mathbf{C}_{\mathrm{ri}}=-\mathbf{C}_{\mathrm{ir}}$. Hence, (10) becomes [12, eq. (7)]

$$\mathbf{C}_{\mathrm{R}}=\begin{bmatrix}\mathbf{C}_{\mathrm{rr}} & \mathbf{C}_{\mathrm{ri}}\\ -\mathbf{C}_{\mathrm{ri}} & \mathbf{C}_{\mathrm{rr}}\end{bmatrix}. \tag{11}$$

The real and imaginary parts of the measurements z are stacked to have a real-valued measurement vector. The posterior formulae in the time are available at [12, eqs. (12) and (13)], and the posterior formulae in the frequency domain are available at (and used in this article) from [12, eqs. (15) and (16)]. The extra covariances required for the frequency-domain posterior are the covariance in the frequency domain ($\mathbf{C}_{\mathrm{FF}}$) and the cross-covariance between the time and frequency domain ($\mathbf{C}_{\mathrm{tF}}$).

For the time covariance model of (6), the $\mathbf{C}_{\mathrm{FF}}$ is given by [12, eq. (24)]

$$\begin{aligned}C_{\mathrm{FFrr}}(f_p,f_q)&=\frac{1}{2}\mathcal{FT}(C(\tau))\left(\frac{f_p+f_q}{2}\right)\delta(f_p-f_q)\\&=\sum_{q=1}^{Q}\frac{P_q}{2\sqrt{2\pi\sigma_{q,fn}^2}}\exp\left[-\frac{\left(\frac{f_p+f_q}{2}-\mu_{q,fn}\right)^2}{2\sigma_{q,fn}^2}\right]\\&\quad\times\delta(f_p-f_q),\\C_{\mathrm{FFri}}(f_p,f_q)&=0\end{aligned} \tag{12}$$

where the operator $\mathcal{FT}$ is the Fourier transform operator, and δ is the Dirac delta function; making it a diagonal matrix. It is also the power spectral density (PSD) of the signal model. The matrix $\mathbf{C}_{\mathrm{tF}}$ is given by [12, eq. (21)]

$$\begin{aligned}C_{\mathrm{tFrr}}(t,f)&=\frac{1}{2}\mathcal{FT}(C(\tau))(f)\cos(2\pi ft)\\&=\sum_{q=1}^{Q}\frac{P_q}{2\sqrt{2\pi\sigma_{q,fn}^2}}\exp\\&\quad\times\left[-\frac{(f-\mu_{q,fn})^2}{2\sigma_{q,fn}^2}\right]\cos(2\pi ft),\end{aligned} \tag{13}$$

$$\begin{aligned}C_{\mathrm{tFri}}(t,f)&=-\frac{1}{2}\mathcal{FT}(C(\tau))(f)\sin(2\pi ft)\\&=-\sum_{q=1}^{Q}\frac{P_q}{2\sqrt{2\pi\sigma_{q,fn}^2}}\exp\\&\quad\times\left[-\frac{(f-\mu_{q,fn})^2}{2\sigma_{q,fn}^2}\right]\sin(2\pi ft).\end{aligned} \tag{14}$$

VI. Numerical Simulation

This section presents the performance analysis of the hyperparameter estimation with $Q=1$. The performance metrics are the bias and the variance.

A. Sampling Strategy

The specifications of the log-periodic sampling are given below. The sample time instances of the sampling strategy are given by the following rule:

$$t_{k,\mathrm{ap}}=\frac{d_1}{d_2}\left[\exp(d_2k)-1\right],\quad k=0,1,2,\ldots,N_{\mathrm{ap}}-1. \tag{15}$$

The parameter d_2 is the exponential growth rate of the sequence. If d_2 approaches 0, the sequence resembles a periodic sequence because $\lim_{d_2\to 0}[\exp(d_2k)-1]/d_2=k$. The larger the d_2, the more nonuniform the sequence becomes.

Let us define a periodic sampling sequence adequate enough for a fair comparison. The parameter d_1 is chosen such that the minimum sampling interval of $\Delta t_{k,\mathrm{ap}}$ (i.e., $\Delta t_{k,\mathrm{ap,min}}$) remains greater or equal to the sampling interval of the periodic sampling $t_{k,\mathrm{per}}$ (i.e., $\Delta t_{k,\mathrm{per}}$)

$$d_1\approx\Delta t_{k,\mathrm{per}}. \tag{16}$$

First, this is deliberately posed in this article to have a fair comparison of the performance. By imposing this, we ensure that the number of samples present in the aperiodic case is not greater than the periodic one. The spectral quantities, such as the Doppler moments, are normalized to the Nyquist unambiguous velocity interval $2V_{a,\mathrm{per}}$ associated with this periodic sampling sequence for intuitive performance analysis.

Second, for practical applications involving FMCW radars, this fixed minimum interval between sweeps ensures a desired maximum range and avoids the issues related to the range overlaid signals. In practice, only the field view (maximum unambiguous range) corresponding to this minimum sampling interval can be studied. A practical suggestion regarding the realization of the proposed aperiodic sampling sequence is

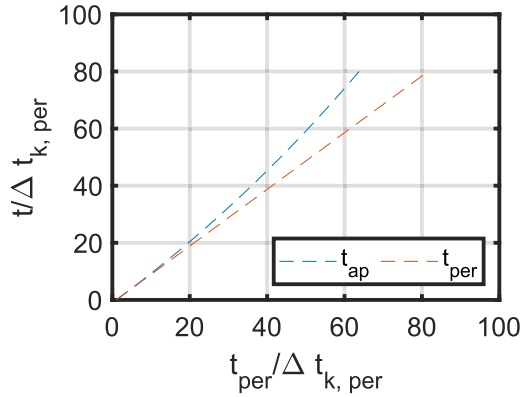

Fig. 1. Sampling sequences: periodic and aperiodic cases.

presented in Section VI-F. We do not study the impact of overlaid signals.

To ensure the same dwell time T, the number of samples in the periodic sequence is typically larger than that of the aperiodic one

$$t_{k,\mathrm{per}} = k\Delta t_{k,\mathrm{per}}, \quad k = 0, 1, 2, \ldots, N_{\mathrm{per}} - 1$$
$$N_{\mathrm{per}} = \left\lceil \frac{T}{\Delta t_{k,\mathrm{per}}} \right\rceil + 1 > N_{\mathrm{ap}}, \quad \forall d_2 > 0. \tag{17}$$

A sequence of $N_{\mathrm{per}} = 82$ samples for the periodic case and $N_{\mathrm{ap}} = 64$ samples for the aperiodic case is shown in Fig. 1 with $d_1 = 1$ and $d_2 = 0.0074$. The decimal point precision in this sampling example is restricted to $D = 3$ for the aperiodic sequence for the performance analysis.

Let us define a staggered sampling sequence as well for comparison. To make a fair comparison, we also choose the minimum spacing between the samples to be greater than $\Delta t_{k,\mathrm{per}}$. To create a staggered sampling sequence with an underlying periodic sequence (with an interval of $10^{-D}\Delta t_{k,\mathrm{per}}$), we have chosen $m = 1001$ and $n = 1502$. The sampling sequence for the staggered case is, therefore,

$$\mathbf{t}_{\mathrm{st}} = [0, 1.001, 2.503, 3.504, \ldots]^{\mathrm{T}} \times \Delta t_{k,\mathrm{per}}. \tag{18}$$

It can be observed from (18) that the staggered sampling sequence has a minimum sampling interval greater than $\Delta t_{k,\mathrm{per}}$ has a decimal point precision of $D = 3$, and a staggered sampling ratio $\Delta t_{1,\mathrm{st}}/\Delta t_{2,\mathrm{st}} = m/n = 1001/1502 \approx 2/3$. The constituent sampling intervals in this staggered sequence are $\Delta t_{1,\mathrm{st}} = 1.001\Delta t_{k,\mathrm{per}}$, and $\Delta t_{2,\mathrm{st}} = 1.502\Delta t_{k,\mathrm{per}}$. The theoretical unambiguous velocity for this sequence is

$$V_{a,\mathrm{ap}} = \frac{\lambda m}{4\Delta t_{1,\mathrm{st}}} = \frac{\lambda n}{4\Delta t_{2,\mathrm{st}}} \approx \frac{10^D}{2\Delta t_{k,\mathrm{per}}} = 10^D V_{\mathrm{a,per}}. \tag{19}$$

The mean Doppler frequency in the case of staggered sampling is estimated using the velocity difference transfer function approach given in [34]. Although the performance shown in [34] is as expected for smaller values of m and n (typically < 100), we deliberately chose higher values for m and n (> 1000) to test the performance when the theoretical maximum unambiguous velocity is much higher than the maximum unambiguous velocity of each constituent sampling sequence.

In Sections VI-B and VI-C, the performance analysis of the parameter estimations is studied with the normalized spectral width parameter σ_{fn} and d_2, respectively.

The performance analysis contains the bias and the standard deviation (square root of the variance) for the estimated parameters $\hat{\Theta}$.

The bias of the parameter is given by

$$\mathbb{B}\left[\hat{\Theta}\right] = \mathbb{E}\left[\hat{\Theta}\right] - \Theta. \tag{20}$$

The variance is computed as follows:

$$\mathbb{V}\left[\hat{\Theta}\right] = \mathbb{E}\left[\left(\hat{\Theta} - \mathbb{E}\left[\hat{\Theta}\right]\right)^2\right]. \tag{21}$$

The expectation of the parameter estimation is performed numerically by Monte Carlo simulations.

The theoretical variances have been implemented and plotted for the CGP approach. The inverse Fisher information matrix is computed for the CGP likelihood (with real-valued covariance), and the diagonal entries of its inverse are considered. The entries of the Fisher information matrix are

$$I_{m,n} = -\mathbb{E}\left[\frac{\partial^2 \log(p(z|\Theta))}{\partial\theta_m \partial\theta_n}\right] = \frac{1}{2}\,\mathrm{Tr}\left(\mathbf{C}_{\mathrm{R}}^{-1}(\Theta)\frac{\partial \mathbf{C}_{\mathrm{R}}(\Theta)}{\partial\theta_m}\mathbf{C}_{\mathrm{R}}^{-1}(\Theta)\frac{\partial \mathbf{C}_{\mathrm{R}}(\Theta)}{\partial\theta_n}\right) \tag{22}$$

where the operator "Tr" refers to the matrix trace. The theoretical variance is, therefore,

$$\mathbb{V}^{\mathrm{Theor}}[\theta_m] = \left(\mathbf{I}^{-1}\right)_{m,m}. \tag{23}$$

The inverse of this Fisher information matrix should not be confused with the unbiased CRB in this case, as the retrievals are not entirely unbiased. However, these theoretical variances converge to the unbiased CRB for an infinite number of echo samples $N \to \infty$ as the estimates are asymptotically unbiased. The biased-CRB limits can also be inferred by studying the bias gradient of the estimator, as shown in [67]. However, this is out of the scope of this article, because a functional form of the bias gradient is harder to achieve.

B. Performance Analysis of Hyperparameter Estimation With σ_{fn}

In this section, the bias and standard deviation for the hyperparameters (Doppler moments) are studied with respect to the normalized spectral width σ_{fn} at a fixed $d_2 = 0.0074$. The normalization here is performed with the unambiguous interval for the periodic case ($\mu_{fn} = \mu_v/(2V_{a,\mathrm{per}})$, $\sigma_{fn} = \sigma_v/(2V_{a,\mathrm{per}})$, where μ_v and σ_v are the denormalized Doppler velocity moments). The total power and the noise standard deviation are considered known quantities in these simulations. As both DFT and PSE use PSD for the estimation, an extended normalized frequency axis is used for a fair comparison. The bias and standard deviation in the estimation of the mean Doppler and Doppler spectrum width are presented in Fig. 2. The number of Monte Carlo simulations performed in this case

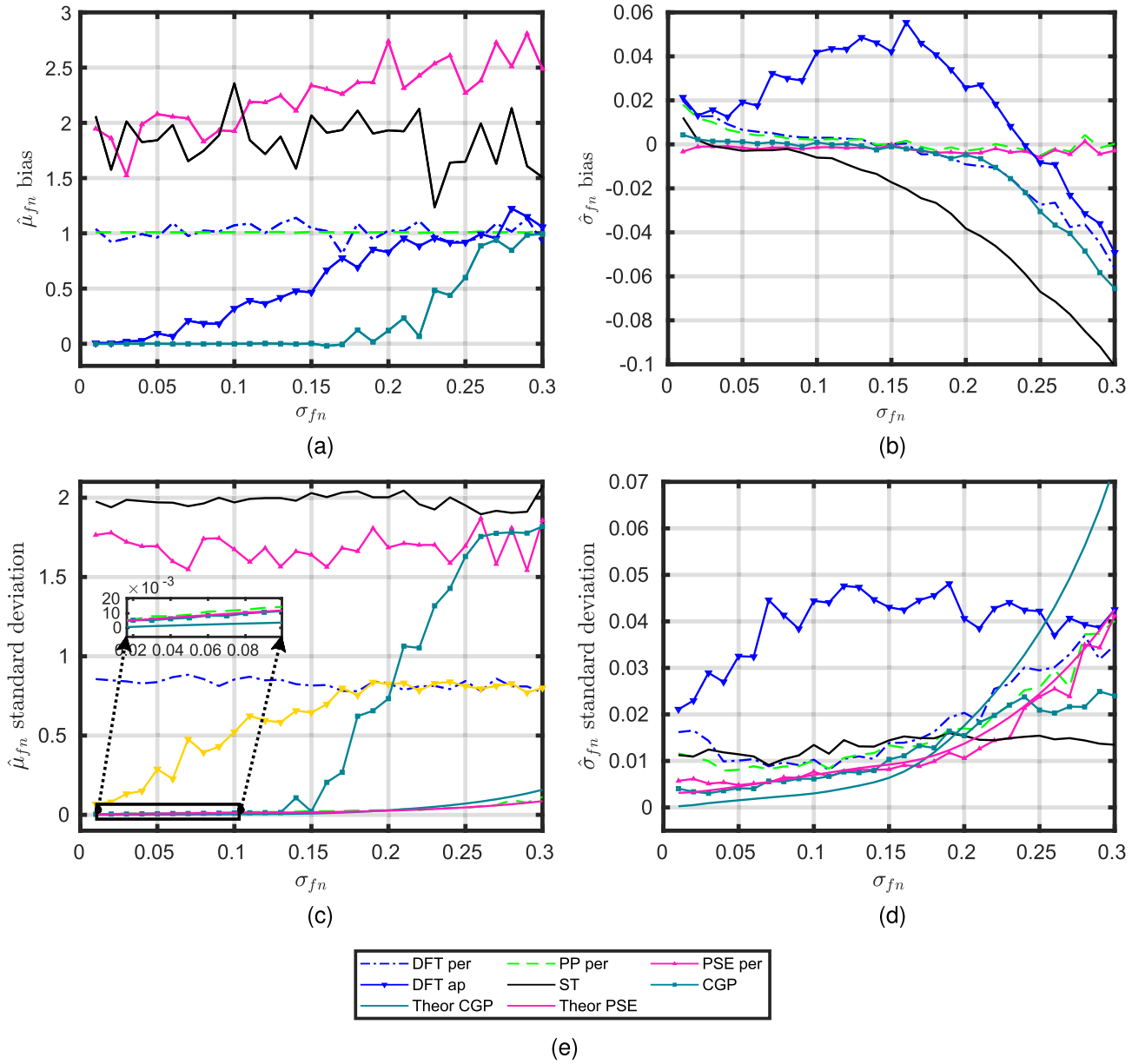

Fig. 2. Estimation and performance of the Doppler moments with respect to σ_{fn}. For the periodic case, the number of samples is 82, whereas for the aperiodic case, it is 64. Bias in estimating (a) mean normalized Doppler frequency $\hat{\mu}_{fn}$ and (b) normalized Doppler frequency width $\hat{\sigma}_{fn}$. Standard deviation in estimating (c) normalized mean Doppler frequency $\hat{\mu}_{fn}$ and (d) normalized Doppler spectrum width normalized $\hat{\sigma}_{fn}$. The abbreviation "per" refers to the periodic sampling, "aper" refers to the aperiodic one, "ST" refers to staggered sampling, and "Theor" refers to the theoretical plots. (e) Legend for the plots.

is 128. The optimization parameters listed in Section IV are set to the following values:

$$\begin{aligned}\left[\mu_{fn,l}, \mu_{fn,u}\right] &= [-3, 3]\\ \left[\sigma_{fn,l}, \sigma_{fn,u}\right] &= [0, 0.5]\\ K &= 256.\end{aligned} \tag{24}$$

In the examples of this article, we chose the parameter space for normalized mean Doppler velocity as three times the Nyquist unambiguous interval for the periodic counterpart.

1) Algorithms Performed on the Periodically Sampled Data: The estimators presented for periodically sampled sequences are DFT, PSE of [11], and the PP algorithm.

The DFT approach of Doppler moment estimation is non-parametric and uses Schuster's periodogram as measurement. It is non-parametric because it assumes no parametric structure of the signal or its Schuster periodogram. The formula mentioned in [15, eq. (9)] is used to compute the mean Doppler frequency (similarly, the square root of the second central moment is computed) for the DFT approach with a known noise variance. For a fair comparison, first, the peak location (frequency at which the power is maximum) of the Schuster periodogram is detected, and one Nyquist unambiguous interval is chosen by keeping this location at the center.

The PSE algorithm is a parametric moment estimator that uses a parametric semianalytical model for the expected Doppler PSD. We chose to use PSE on the PSD of a periodic sequence because the semianalytical model of the PSD [11, eq. (10)] has a lower bias when dealing with periodic

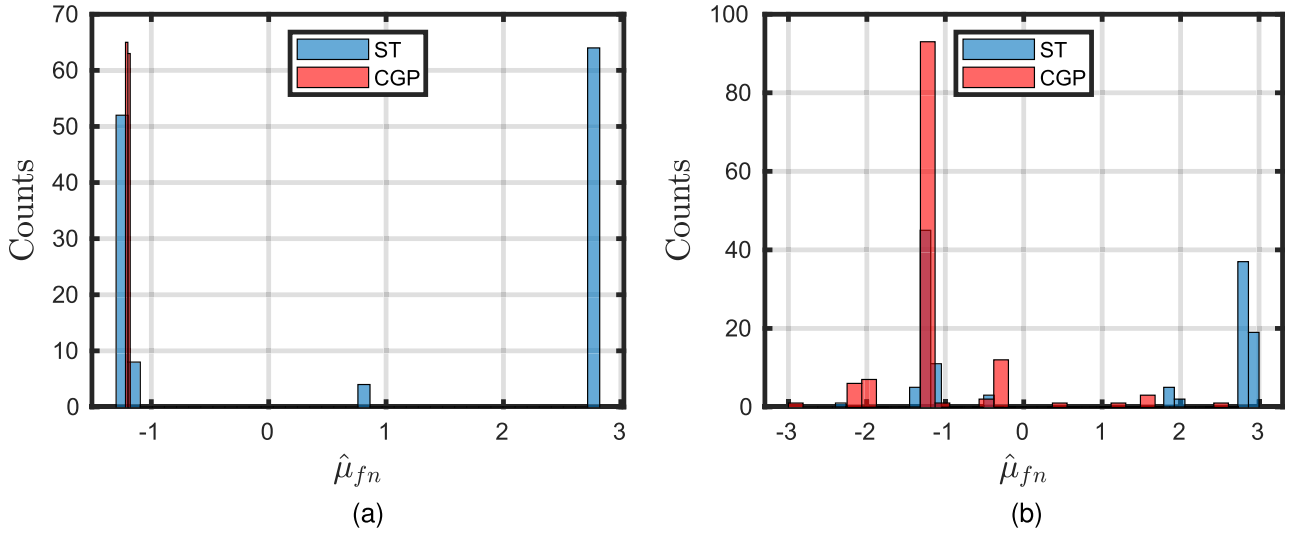

Fig. 3. Histogram of parameter estimates $\hat{\mu}_{fn}$ for staggered ("ST") and the proposed CGP approach at (a) $\sigma_{fn} = 0.01$ and (b) $\sigma_{fn} = 0.1$. True mean Doppler velocity is $\mu_{fn} = -1.2$.

sequences (because it considers the time on target in the model of the PSD as well). The performance analysis in [11] shows that the PSE is more accurate than Levin's approach (which uses a closed form of the Doppler PSD [68] without the time on target). Therefore, we do not study the performance using Levin's approach.

The PP estimates of the Doppler moments are based on the signal's autocorrelation with integer time lags. It is used on a periodic sequence where contiguous pairs can be found. The estimation of mean Doppler with the PP approach is used from [15, eq. (16)]. For the Doppler spectrum width (PP R0/R1), the formula [16, eq. (6.17)] is used as this estimator is asymptotically unbiased.

2) Algorithms Performed on the Aperiodically Sampled Data: A DFT moment estimator is implemented on the Schuster periodogram computed for the aperiodically sampled data with log-periodic sampling. A similar approach with the peak location detection is performed for a fair comparison, as in the periodic case. The moments are computed using this as the frequency window with the DFT approach. The proposed CGP approach has also been implemented on the aperiodically sampled data with log-periodic sampling.

For the staggered sampling case, the de-aliasing approach based on the velocity difference transfer function is used to compute the mean Doppler frequency [34]. To compute the de-aliased mean Doppler frequency, the individual mean Doppler frequencies corresponding to the two constituent periodic sampling sequences need to be estimated first. These mean frequencies [14, eqs. (5.a) and (5.b)] are estimated by the PP approach, but the one-lag autocorrelation can only be performed on independent pairs [14, eqs. (3) and (4)] (contiguous pairs are not available in the case of a staggered sampling sequence). The Doppler spectrum width for the staggered sampling is computed using only one constituent sampling (the smaller one) [14, eq. (6)] using the PP technique.

The true normalized mean Doppler frequency with which the simulation of the signals is carried out is $\mu_{fn} = -1.2$. The noise is added with an input SNR of 12 dB [69].

3) Performance Analysis: It can be observed that the "DFT aperiodic" technique for the mean Doppler estimation has a small bias for extremely small normalized spectral widths. This validates the results in the literature for the periodogram techniques because a very small normalized spectral width is analogous to having one sinusoid in the signal. The nonuniform Schuster periodogram peak detection becomes increasingly ambiguous with increased spectral width.

The periodic counterparts, including the PP algorithm, also show biased results because of aliasing.

In contrast to all these approaches, the proposed CGP approach has a much smaller bias in the normalized mean Doppler frequency estimates for normalized spectral widths less than 0.2. For larger normalized spectral widths, the estimates become increasingly biased because the optimized mean Doppler frequency becomes truly ambiguous and is highly sensitive to the measurement.

The normalized spectral width estimates follow a similar trend in terms of bias for the proposed CGP approach. The PP approach has a smaller bias in the higher normalized spectral width regions. The PSE has the smallest bias across all normalized spectral widths. It has also been shown in [11].

The standard deviation for normalized spectral width of $\sigma_{fn} > 0.3$ is not shown as the results of all estimators are increasingly biased. For the normalized mean Doppler frequency, the proposed approach has lower standard deviations than all the other approaches except for the PP below a normalized spectral width of less than 0.16. PP has the smallest standard deviation because it does not consider an extended frequency axis. Therefore, the estimation result is always near the fixed aliased frequency inside the bound $[-0.5, 0.5]$. The periodic approaches of DFT and PSE have a more significant standard deviation.

All the methods work similarly to the estimation of normalized spectral width except the DFT aperiodic approach.

The theoretical variances for CGP are smaller than the numerical ones for the mean Doppler μ_{fn}. The theoretical variance for the spectral width σ_{fn} is higher than the numerical

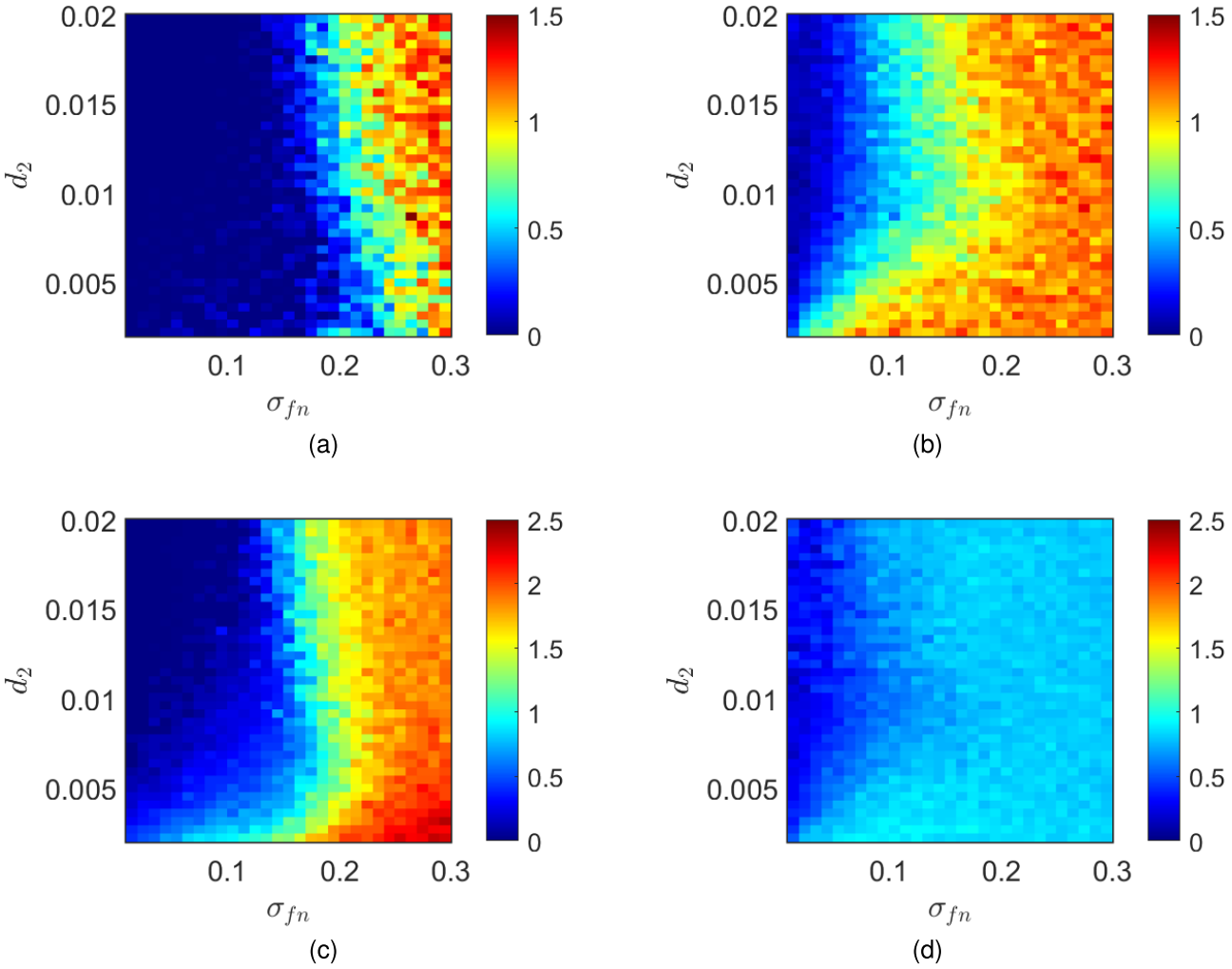

Fig. 4. Estimation and performance of the normalized mean Doppler frequency $\hat{\mu}_{fn}$ with respect to σ_{fn} and d_2. The number of samples is 33. Bias in estimating the mean normalized Doppler frequency $\hat{\mu}_{fn}$. (a) CGP. (b) DFT aperiodic. Standard deviation in estimating the mean normalized Doppler frequency $\hat{\mu}_{fn}$. (c) CGP. (d) DFT aperiodic.

one if $\sigma_{fn} > 0.16$. The differences between the numerical and theoretical variances can be explained by the principles of biased CRB. However, as explained earlier in this section, we do not study the biased CRBs.

The staggered sampling technique also suffers from a large bias for the normalized mean Doppler frequency. The reason for the large bias can be attributed to the fact that the values of m and n are large, although the ratio $m/n \approx 2/3$. It shows the limitation of the staggered sampling technique when the desired theoretical Nyquist unambiguous velocity is much larger than the Nyquist unambiguous velocity of the individual constituent periodic sequences. For large values of m and n (> 1000), to avoid errors, there are recommendations suggested in [34]. However, these suggestions need manual intervention and additional information based on continuity in space and time. Therefore, we did not implement all the suggestions for such a configuration. However, we have noticed that the algorithm successfully estimates the true Doppler velocity almost half of the time across the Monte Carlo simulations. Therefore, instead of only bias and standard deviations in the estimates, we show the distribution (in terms

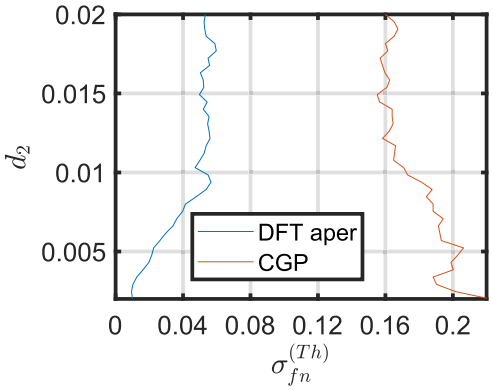

Fig. 5. Spectral width at which $|\mathbb{B}[\hat{\mu}_{fn}]| = 0.24$ as a function of the nonlinearity in the sampling (d_2).

of histograms) of the estimated normalized mean Doppler frequency by both the staggered sampling technique and the proposed CGP technique at normalized Doppler spectrum widths of σ_{fn} of 0.01 and 0.1 in Fig. 3. The comparison with the staggered sampling approach shows that the proposed

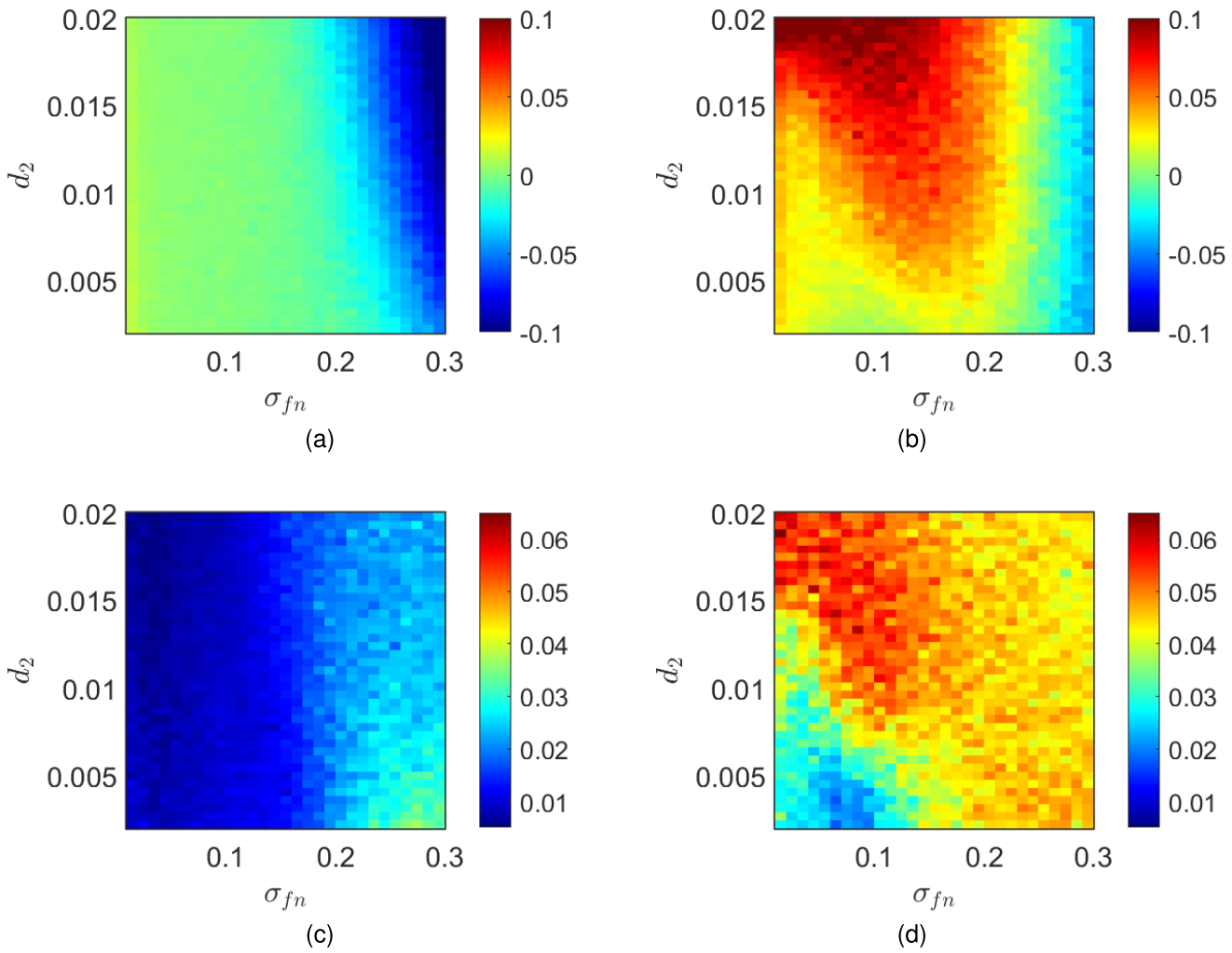

Fig. 6. Estimation and performance of the normalized Doppler spectrum width $\hat{\sigma}_{fn}$ with respect to σ_{fn} and d_2. The number of samples is 33. Bias in estimating the mean normalized Doppler frequency $\hat{\sigma}_{fn}$. (a) CGP. (b) DFT aperiodic. Standard deviation in estimating the mean normalized Doppler frequency $\hat{\sigma}_{fn}$. (c) CGP. (d) DFT aperiodic.

CGP approach is robust against different realizations of the measurements.

The histograms suggest that the proposed CGP approach is distributed around the true normalized mean Doppler frequency, and the width of this distribution increases with an increase in the normalized spectral width. However, the mean of this distribution is closer to the true normalized mean Doppler frequency. In the case of staggered sampling, the distribution is more discrete and only around half of the estimates are around the true value. Therefore, the mean of all the estimates is far away from the true value, causing a larger bias in the estimates. For the Doppler spectrum width, however, the absolute bias is below 0.02 for smaller normalized spectral widths $\sigma_{fn} < 0.16$, indicating good performance. However, overall, the bias of the proposed CGP approach is smaller than that of the staggered PRT approach.

C. Performance Analysis of Hyperparameter Estimation With d_2 for the Aperiodically Sampled Sequence

In this section, we present the performance analysis results of the hyperparameter estimation with both the normalized spectral width σ_{fn} and the nonlinearity in the aperiodic sampling sequence d_2. The value of d_1 is 1 and number of samples N_{ap} is 33 for this analysis. We have chosen the DFT-aperiodic approach for the comparison. The results are shown in Fig. 4 for the normalized mean Doppler frequency.

It can be observed that the bias of $\hat{\mu}_{fn}$ decreases with increasing nonlinearity d_2 for smaller spectral widths. It can also be observed that the spectral width at which the absolute bias starts to rise for CGP decreases with an increase in d_2. This implies a trade-off between the spectral width at which $\hat{\mu}_{fn}$ gets increasingly biased and the estimator's accuracy for smaller spectral widths. To demonstrate this, Fig. 5 shows the location of the σ_{fn} (represented as $\sigma_{fn}^{(\text{Th})}$) at which the bias of $\hat{\mu}_{fn}$ reaches a threshold that is 20% of its true value. In this analysis, the true $\mu_{fn} = -1.2$, and the threshold for the absolute bias is $|\mathbb{B}[\hat{\mu}_{fn}]| = 0.24$. It can be observed that the $\sigma_{fn}^{(\text{Th})}$ is converging to 0.16 with increasing d_2. The values of $\sigma_{fn}^{(\text{Th})}$ for the DFT aperiodic approach are much smaller than the proposed CGP approach, indicating the superiority of CGP for applications involving extended targets (larger spectral widths).

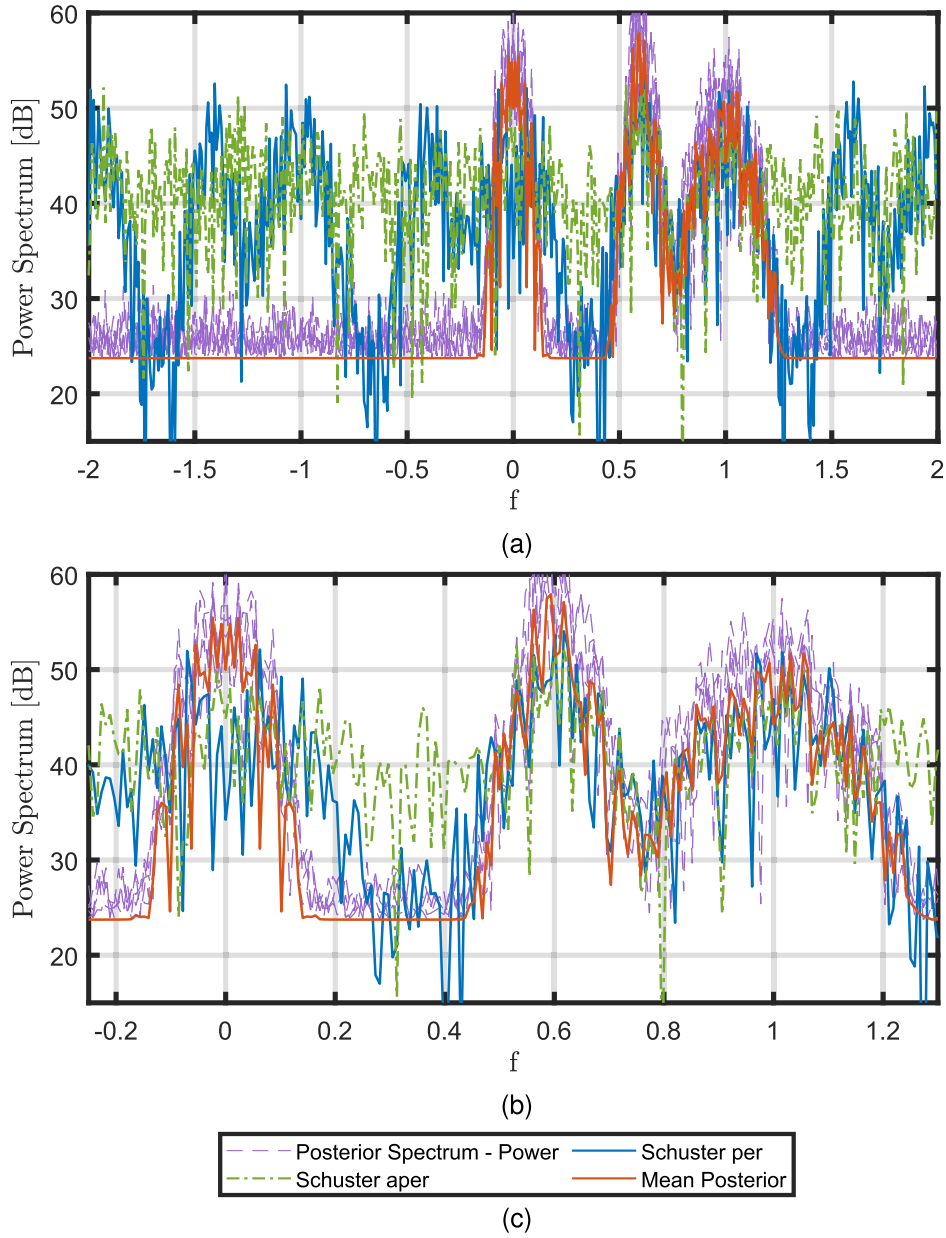

Fig. 7. Spectrum reconstruction: (a) power spectrum, (b) power spectrum zoomed in, and (c) legend for the plots. The posterior spectrum contains five realizations of the power spectrum.

The standard deviation for $\hat{\mu}_{fn}$ of the DFT aperiodic approach has much smaller values than the proposed CGP approach because of its rigid biased nature due to aliasing (for $\sigma_{fn} > 0.1$).

The performance analysis for the normalized Doppler spectrum width is shown in Fig. 6.

For the spectral width estimation, the bias of the proposed CGP approach is nearly zero for $\sigma_{fn} < 0.16$ for all values of d_2. The proposed approach is superior and less biased than the DFT aperiodic approach. The standard deviation of CGP approach for $\hat{\sigma}_{fn}$ is smaller than that of the DFT-aperiodic approach with increasing d_2. For $\sigma_{fn} > 0.16$, with increasing d_2, the standard deviation of CGP is smaller than that of the DFT aperiodic approach.

D. Recommendation for Minimum Pulse Repetition Interval

With the abovementioned analysis, it can be concluded that for a normalized spectral width less than 0.16, the proposed approach produces unambiguous Doppler moments for a precipitation-like extended target. Therefore, we recommend using the log-periodic sampling with a minimum sampling interval ($\Delta t_{\text{ap,min}}$), which satisfies the following relationship:

$$\frac{\lambda}{2\Delta t_{\text{ap,min}}} \geq 6\sigma_v \tag{25}$$

which implies

$$\Delta t_{\text{ap,min}} \leq \frac{\lambda}{12\sigma_v}. \tag{26}$$

TABLE I
HYPERPARAMETER ESTIMATION

Parameter	True	Estimated
$\mu_{1,fn}$	1	1.002
$\mu_{2,fn}$	0.6	0.6053
$\sigma_{1,fn}$	0.09	0.0881
$\sigma_{2,fn}$	0.06	0.0513
$\sigma_{3,fn}$	0.02	0.0161
P_1	10000	10120
P_2	10000	99424
P_3	1000	700

Here, λ is the radar central wavelength, and σ_v is the extended target's absolute, denormalized Doppler spectral width. The choice of σ_v depends on the application.

E. Simulation Study of the Spectrum Reconstruction

Three extended targets are used to simulate the radar echoes in time. Two of these extended targets mimic two precipitation-like targets. The mean locations of these two targets are kept outside the Nyquist unambiguous interval of the periodic sampling case purposefully to evaluate the retrieval and reconstruction. The third extended target is a clutter whose mean location is $\mu_{3,fn} = 0$, which is assumed to be a known quantity. The unknown hyperparameters are $\Theta = [\mu_{1,fn}, \mu_{2,fn}, \sigma_{1,fn}, \sigma_{2,fn}, \sigma_{3,fn}, P_1, P_2, P_3]$. The number of echo samples for the periodic case is $N_{\text{per}} = 213$, and for the aperiodic case is $N_{\text{ap}} = 128$. The parameters for the aperiodic sequence are $d_1 = 1$ and $d_2 = 0.0074$.

The hyperparameter estimation is shown in Table I. The spectrum reconstruction is then followed using the principles mentioned in Section V.

As it is a Bayesian approach, we present several different realizations of the power spectrum in Fig. 7 by first sampling from the posterior distributions of its real and imaginary parts, respectively.

It can be concluded that the proposed CGP-based reconstruction avoids the ambiguous responses of the extended targets in the extended frequency domain by the counter-aliasing strategy. The reconstruction in the frequency domain is performed using the measurements in the time domain, posing no additional computational burden. The Schuster periodogram with the periodic sequence has produced an aliased Doppler spectrum in the extended frequency domain, making it uninformative. Likewise, the Schuster periodogram with the aperiodic sequence (same as the generalized Lomb–Scargle periodogram) has produced very high levels of artifacts (comparable with the power of the real targets), making it ambiguous. However, the CGP posterior avoids these ambiguous artifacts and has smaller sidelobe levels (around 35 dB) in this case. Therefore, there is an improvement of around 20 dB over the other approaches as far as the ambiguous artifact levels are concerned.

F. Recommendations for Real Radar Application

An application to real radar measurements with this proposed setting should be studied. Changing the reset time $T_k^{(\text{reset})}$ aperiodically by applying the sampling rules for a frequency modulated continuous wave (FCMW) radar can be beneficial in realizing such a configuration. The reset time is the time difference between the end of one chirp and the start of the next. The chirp duration $T^{(\text{chirp})}$ is constant and is very less than $\Delta t_{k,\text{per}}$

$$\begin{aligned} T_k^{(\text{reset})} &= t_k\left(\Delta t_{k,\text{per}}, d_1, d_2\right) - t_{k-1}\left(\Delta t_{k,\text{per}}, d_1, d_2\right) \\ &\quad - T^{(\text{chirp})} \\ T^{(\text{chirp})} &\ll \Delta t_{k,\text{per}}. \end{aligned} \tag{27}$$

A constant reset time (when $t_k(\Delta t_{k,\text{per}}, d_1, d_2) - t_{k-1}(\Delta t_{k,\text{per}}, d_1, d_2) = \Delta t_{k,\text{per}}$) will redirect the radar to the periodic pulse repetition mode.

The software used in the simulation studies was written with the help of Matrix Laboratory (MATLAB) optimization toolbox [70] on a Linux platform. The optimization is performed by the constrained optimization tool ("fmincon") of MATLAB with options given in Section IV. As this tool is a local minima finder, we have used the negative log-likelihood as the fitness (cost) function.

VII. CONCLUSION

This article proposes a novel integrative Doppler counter-aliasing signal processing strategy for precipitation-like extended targets using aperiodically sampled radar echoes in time.

Although the existing signal processing approaches have addressed the issues related to aliasing/ambiguity in the Doppler spectrum, the research gaps have been explicitly stated in various research areas. After assessing these research gaps carefully, a novel counter-aliasing strategy is proposed for extended targets like precipitation.

We do a novel study on the effect of aperiodic sampling on the statistics of the Doppler parameter estimation for precipitation-like extended targets. We propose to apply CGP regression to aperiodically sampled signals. Using this parametric technique, we estimate the parameters first and then reconstruct the Doppler spectrum. The advantage of such aperiodic sampling over its periodic counterparts is that the maximum observable frequency (in the context of this article, it is the maximum unambiguous Doppler frequency or velocity) is much higher. The results with the aperiodically sampled signal are compared with a periodic sampling case with a sampling time shorter than the minimum sampling time of the aperiodic case for a fair comparison. For a large range of normalized Doppler spectrum widths, the proposed approach can accurately estimate the mean Doppler velocity when the true mean Doppler velocity is larger than the unambiguous velocity of its periodic counterpart. The aperiodic sequence proposed in this article is also compared with a state-of-the-art staggered sampling sequence. A post-processing de-aliasing algorithm is performed on the staggered sequence, and the results of the Doppler moments estimation are compared with the proposed approach. The proposed approach is found to be superior to the staggered sampling algorithm in terms of the bias in the estimates.

We propose a novel criterion for designing a log-periodic sampling sequence with a minimum sampling interval lower than $\lambda/(12 \times \sigma_v)$ (where the spectral width σ_v is related to the storm's severity) for an unambiguous retrieval of the mean Doppler velocity. The more severe the storm in terms of spectral width (which can result from strong turbulence, vortices, and convective storms), the smaller the minimum sampling interval needed.

In addition, this article presents a Bayesian inference approach to reconstructing the Doppler spectrum with an extended velocity domain by directly using the aperiodically sampled echoes in the time domain. The reconstruction poses no additional computational burden. As it is a Bayesian technique, we get several different realizations of the power spectrum. To the authors' knowledge, this is the first-ever implementation of the direct frequency-domain Gaussian process posterior on aperiodically sampled sequences for extended targets, making it novel. The mean estimate of the power spectrum converges to the true spectrum. It is shown that the posterior spectrum of the proposed reconstruction outperforms the conventional periodogram techniques capable of handling aperiodic signals, such as the aperiodic Schuster periodogram, in terms of accuracy. The problem of higher ambiguous artifacts is avoided using the proposed approach. It has been shown in Fig. 7 that there is at least 20 dB improvement in the ambiguous artifact levels.

This study does not include the impact of such a pulse train on estimating the target's range. However, as with the log-periodic sampling technique, the minimum sampling interval in the slow time can be maintained at a desired level, which can decide the maximum unambiguous range to which the mean Doppler velocity and Doppler spectrum width can be recovered.

In addition, more theoretical statistical studies should be carried out for the performance analysis of random processes having Gaussian mixture-type covariance functions. The Gaussian mixture (with two or more targets) type covariance functions are useful to model the response from severe weather conditions. The performance of parameter estimation for Gaussian mixture models (GMM) is highly sensitive to the distance between the means of any two individual Gaussian components and their spectral widths.

ACKNOWLEDGMENT

The authors would like to thank Ir. Abdul Syed Mohamed, for his insightful and thought-provoking analysis of log-periodic sampling explained in his master's thesis (see [45]). They also thank the anonymous reviewers for their meticulous reviews, which improved the manuscript.

REFERENCES

[1] S. Yuan, P. Aubry, F. Fioranelli, and A. G. Yarovoy, "A novel approach to unambiguous Doppler beam sharpening for forward-looking MIMO radar," *IEEE Sensors J.*, vol. 22, no. 23, pp. 23494–23506, Dec. 2022.

[2] S. Yuan, F. Fioranelli, and A. G. Yarovoy, "3DRUDAT: 3D robust unambiguous Doppler beam sharpening using adaptive threshold for forward-looking region," *IEEE Trans. Radar Syst.*, vol. 2, pp. 138–153, 2024.

[3] B. Yang, S. Liu, H. Zhang, and Y. Zhou, "A velocity ambiguity resolution algorithm based on improved hypothetical phase compensation for TDM-MIMO radar traffic target imaging," *IEEE J. Sel. Topics Appl. Earth Observ. Remote Sens.*, vol. 17, pp. 3409–3424, 2024. [Online]. Available: https://ieeexplore.ieee.org/document/10387688/

[4] S. Chen, Y. Yuan, S. Zhang, H. Zhao, and Y. Chen, "A new imaging algorithm for forward-looking missile-borne bistatic SAR," *IEEE J. Sel. Topics Appl. Earth Observ. Remote Sens.*, vol. 9, no. 4, pp. 1543–1552, Apr. 2016.

[5] M. Zhang, G. Liao, X. He, and S. Zhu, "Unambiguous forward-looking SAR imaging on HSV-R using frequency diverse array," *Sensors*, vol. 20, no. 4, p. 1169, Feb. 2020.

[6] Y. Zhang, D. Mao, Y. Zhang, Y. Huang, and J. Yang, "Multi-beam Doppler beam sharpening approach for airborne forward-looking radar imaging," in *Proc. IEEE Int. Geosci. Remote Sens. Symp. (IGARSS)*, Jul. 2017, pp. 6142–6145.

[7] S. Muth, S. Dort, I. A. Sebag, M.-J. Blais, and D. Garcia, "Unsupervised dealiasing and denoising of color-Doppler data," *Med. Image Anal.*, vol. 15, no. 4, pp. 577–588, Aug. 2011.

[8] H. Nahas, J. S. Au, T. Ishii, B. Y. S. Yiu, A. J. Y. Chee, and A. C. H. Yu, "A deep learning approach to resolve aliasing artifacts in ultrasound color flow imaging," *IEEE Trans. Ultrason., Ferroelectr., Freq. Control*, vol. 67, no. 12, pp. 2615–2628, Dec. 2020.

[9] A. Oglat, M. Matjafri, N. Suardi, M. Oqlat, M. Abdelrahman, and A. Oqlat, "A review of medical Doppler ultrasonography of blood flow in general and especially in common carotid artery," *J. Med. Ultrasound*, vol. 26, no. 1, p. 3, 2018.

[10] T. Dash, O. A. Krasnov, and A. G. Yarovoy, "Performance analysis of the wind field estimation for a very fast scanning weather radar," in *Proc. 23rd Int. Radar Symp. (IRS)*, Sep. 2022, pp. 420–425.

[11] T. Dash, H. Driessen, O. Krasnov, and A. Yarovoy, "Doppler spectrum parameter estimation for weather radar echoes using a parametric semianalytical model," *IEEE Trans. Geosci. Remote Sens.*, vol. 62, 2024, Art. no. 5100218.

[12] T. Kumar Dash, H. Driessen, O. Krasnov, and A. Yarovoy, "Precipitation Doppler spectrum reconstruction with Gaussian process prior," in *Proc. IEEE Conf. Antenna Meas. Appl. (CAMA)*, Nov. 2023, pp. 909–914.

[13] P. R. Mahapatra and D. S. ZrniC, "Practical algorithms for mean velocity estimation in pulse Doppler weather radars using a small number of samples," *IEEE Trans. Geosci. Remote Sens.*, vol. GE-21, no. 4, pp. 491–501, Oct. 1983.

[14] D. S. Zrnic, "Spectral moment estimates from correlated pulse pairs," *IEEE Trans. Aerosp. Electron. Syst.*, vol. AES-13, no. 4, pp. 344–354, Jul. 1977.

[15] D. Sirmans and B. Bumgarner, "Numerical comparison of five mean frequency estimators," *J. Appl. Meteorol. Climatol.*, vol. 14, no. 6, pp. 991–1003, Sep. 1975.

[16] E. G. Baxa and J. Lee, "The pulse-pair algorithm as a robust estimator of turbulent weather spectral parameters using airborne pulse Doppler radar," NASA, Tech. Rep. NASA-CR-4382, DOT/FAA/RD-91/17, 1991.

[17] P. T. May, T. Sato, M. Yamamoto, S. Kato, T. Tsuda, and S. Fukao, "Errors in the determination of wind speed by Doppler radar," *J. Atmos. Ocean. Technol.*, vol. 6, no. 2, pp. 235–242, Apr. 1989. [Online]. Available: http://journals.ametsoc.org/doi/10.1175/1520-0426(1989)006%3C0235:EITDOW%3E2.0.CO;2

[18] A. Oude Nijhuis, "Radar remote sensing of wind vector and turbulence intensity fields from raindrop backscattering," Ph.D. dissertation, Dept. Microelectron., Delft Univ. Technol., Delft, The Netherlands, 2019. [Online]. Available: https://doi.org/10.4233/uuid:a992351f-c72e-4b7f-9162-f625eed0dcdd

[19] F. J. Yanovsky, H. W. J. Russchenberg, L. P. Ligthart, and Y. A. Aver'yanova, "Model of drop canting in microwave remote sensing of rain," in *Proc. 4th Int. Kharkov Symp. 'Phys. Eng. Millim. Sub-Millim. Waves'*, Jun. 2001, pp. 471–473.

[20] F. J. Yanovsky, I. G. Prokopenko, K. I. Prokopenko, H. W. J. Russchenberg, and L. P. Ligthart, "Radar estimation of turbulence eddy dissipation rate in rain," in *Proc. IEEE Int. Geosci. Remote Sens. Symp.*, Jun. 2002, pp. 63–65.

[21] F. J. Yanovsky, H. W. J. Russchenberg, and C. M. H. Unal, "Retrieval of information about turbulence in rain by using Doppler-polarimetric radar," *IEEE Trans. Microw. Theory Techn.*, vol. 53, no. 2, pp. 444–450, Feb. 2005.

[22] P. Borque, E. Luke, and P. Kollias, "On the unified estimation of turbulence eddy dissipation rate using Doppler cloud radars and LiDARs," *J. Geophys. Res., Atmos.*, vol. 121, no. 10, pp. 5091–6129, 2016.

[23] K. Browning and R. Wexler, "The determination of kinematic properties of a wind field using Doppler radar," *J. Appl. Meteorol. Climatol.*, vol. 7, no. 1, pp. 105–113, 1968.

[24] C. Qiu and Q. Xu, "A simple adjoint method of wind analysis for single-Doppler data," *J. Atmos. Ocean. Technol.*, vol. 9, no. 5, pp. 588–598, 1992.

[25] A. Shapiro, S. Ellis, and J. Shaw, "Single-Doppler velocity retrievals with Phoenix II data: Clear air and microburst wind retrievals in the planetary boundary layer," *J. Atmos. Sci.*, vol. 52, no. 9, pp. 1265–1287, May 1995.

[26] C.-J. Qiu and Q. Xu, "Least squares retrieval of microburst winds from single-Doppler radar data," *Monthly Weather Rev.*, vol. 124, no. 6, pp. 1132–1144, Jun. 1996.

[27] Y.-C. Liou, "An explanation of the wind speed underestimation obtained from a least squares type single-Doppler radar velocity retrieval method," *J. Appl. Meteorol.*, vol. 41, no. 7, pp. 811–823, Jul. 2002.

[28] C. J. Qiu, A. M. Shao, S. Liu, and Q. Xu, "A two-step variational method for three-dimensional wind retrieval from single Doppler radar," *Meteorol. Atmos. Phys.*, vol. 91, nos. 1–4, pp. 1–8, 2006.

[29] Y. C. Liou, H. B. Bluestein, M. M. French, and Z. B. Wienhoff, "Single-Doppler velocity retrieval of the wind field in a tornadic supercell using mobile, phased-array, Doppler radar data," *J. Atmos. Ocean. Technol.*, vol. 35, no. 8, pp. 1649–1663, 2018.

[30] V. Louf, A. Protat, R. C. Jackson, S. M. Collis, and J. Helmus, "UNRAVEL: A robust modular velocity dealiasing technique for Doppler radar," *J. Atmos. Ocean. Technol.*, vol. 37, no. 5, pp. 741–758, May 2020.

[31] W. Lu, "User-centric signal processing of high-resolution meteorological phased array radar," M.S. thesis, Delft Univ. Technol., Delft, The Netherlands, 2023. [Online]. Available: http://resolver.tudelft.nl/uuid:7fbb554c-1aa3-4d16-8f13-a16c988f5ff9

[32] C. N. James and J. Houze, "A real-time four-dimensional Doppler dealiasing scheme," *J. Atmos. Ocean. Technol.*, vol. 18, no. 10, pp. 1674–1683, 2001.

[33] Q. Xu and C. Qiu, "Adjoint-method retrievals of low-altitude wind fields from single-Doppler reflectivity and radial-wind data," *J. Atmos. Ocean. Technol.*, vol. 12, no. 5, pp. 1111–1119, 1995.

[34] S. M. Torres, Y. F. Dubel, and D. S. Zrnić, "Design, implementation, and demonstration of a staggered PRT algorithm for the WSR-88D," *J. Atmos. Ocean. Technol.*, vol. 21, no. 9, pp. 1389–1399, 2004.

[35] S. M. Torres and D. A. Warde, "Staggered-PRT sequences for Doppler weather radars. Part I: Spectral analysis using the autocorrelation spectral density," *J. Atmos. Ocean. Technol.*, vol. 34, no. 1, pp. 51–63, Jan. 2017. [Online]. Available: https://journals.ametsoc.org/view/journals/atot/34/1/jtech-d-16-0071.1.xml

[36] D. Schvartzman and R. D. Palmer, "Doppler velocity recovery and dealiasing algorithm for multi-PRT scans in weather radars," *IEEE Trans. Geosci. Remote Sens.*, vol. 62, 2024, Art. no. 5106514.

[37] J. T. VanderPlas, "Understanding the Lomb–Scargle periodogram," *Astrophys. J. Suppl.*, vol. 236, no. 1, p. 16, 2018, doi: 10.3847/1538-4365/aab766.

[38] A. W. Doerry, "Radar Doppler processing with nonuniform PRF," Sandia Nat. Laboratories Albuquerque, Albuquerque, NM, USA, Tech. Rep. SAND2017-7851, 2017. [Online]. Available: https://www.osti.gov/servlets/purl/1373645

[39] F. Particke, A. Schmidt, C. Rügheimer, and T. Mahr, "Additive random sampling for radar signal processing," in *Proc. IEEE-APS Top. Conf. Antennas Propag. Wireless Commun. (APWC)*, Sep. 2017, pp. 93–96.

[40] M. W. Maciejewski, H. Z. Qui, I. Rujan, M. Mobli, and J. C. Hoch, "Nonuniform sampling and spectral aliasing," *J. Magn. Reson.*, vol. 199, no. 1, pp. 88–93, Jul. 2009.

[41] C. J. Ryan, W. L. Beardell, J. Murakowski, D. D. Ross, G. J. Schneider, and D. W. Prather, "Log-periodic temporal apertures for grating lobe suppression in k-space tomography," *Opt. Exp.*, vol. 28, no. 11, pp. 15969–15983, 2020.

[42] A. Schuster, "On the investigation of hidden periodicities with application to a supposed 26 day period of meteorological phenomena," *Terr. Magn.*, vol. 3, no. 1, pp. 13–41, 1898.

[43] Y. Aslan, "Optimization of virtually aperiodic linear sparse arrays," *Microw. Opt. Technol. Lett.*, vol. 64, no. 2, pp. 318–324, Feb. 2022.

[44] M. Xu, C. Zhang, H. Qiao, Q. Zhang, C. Deng, and W. Yu, "Sparse antenna array with flat-top and sharp cutoff radiation patterns," *IEEE Trans. Antennas Propag.*, vol. 71, no. 6, pp. 4695–4703, Jun. 2023.

[45] S. A. Kader, "De-aliasing of Doppler spectrum for a fast scanning phased array radar," M.S. thesis, Delft Univ. Technol., Delft, The Netherlands, 2023. [Online]. Available: http://resolver.tudelft.nl/uuid:6313a6ec-c14f-4590-a488-bc620904d95e

[46] T. Yardibi, J. Li, P. Stoica, M. Xue, and A. B. Baggeroer, "Source localization and sensing: A nonparametric iterative adaptive approach based on weighted least squares," *IEEE Trans. Aerosp. Electron. Syst.*, vol. 46, no. 1, pp. 425–443, Jan. 2010.

[47] P. Stoica, E. G. Larsson, and J. Li, "Adaptive filter-bank approach to restoration and spectral analysis of gapped data," *Astronomical J.*, vol. 120, no. 4, pp. 2163–2173, Oct. 2000.

[48] A. Mortier, J. P. Faria, C. M. Correia, A. Santerne, and N. C. Santos, "BGLS: A Bayesian formalism for the generalised Lomb-Scargle periodogram," *Astron. Astrophys.*, vol. 573, p. 24908, Jan. 2015.

[49] J. Wang, M. Ding, and A. Yarovoy, "Matrix-pencil approach-based interference mitigation for FMCW radar systems," *IEEE Trans. Microw. Theory Techn.*, vol. 69, no. 11, pp. 5099–5115, Nov. 2021.

[50] E. T. Jaynes and G. L. Bretthorst, *Probability Theory: The Logic of Science*. Cambridge, U.K.: Cambridge Univ. Press, 2003.

[51] N. J. Bartlett, C. Renton, and A. G. Wills, "An improved random matrix prediction model for manoeuvring extended targets," 2021, *arXiv:2105.12299*.

[52] G. L. Bretthorst, "Generalizing the Lomb-Scargle periodogram—The nonsinusoidal case," in *Proc. AIP Conf.*, vol. 568, 2001, pp. 246–251.

[53] R. Boloix-Tortosa, F. Javier Payán-Somet, E. Arias-de-Reyna, and J. José Murillo-Fuentes, "Proper complex Gaussian processes for regression," 2015, *arXiv:1502.04868*.

[54] F. Tobar, "Bayesian nonparametric spectral estimation," in *Proc. Adv. Neural Inf. Process. Syst.*, 2018, pp. 10127–10137.

[55] Y. Wang, R. Khardon, and P. Protopapas, "Nonparametric Bayesian estimation of periodic light curves," *Astrophys. J.*, vol. 756, no. 1, p. 67, 2012.

[56] M. Fang, R. J. Doviak, and V. Melnikov, "Spectrum width measured by WSR-88D: Error sources and statistics of various weather phenomena," *J. Atmos. Ocean. Technol.*, vol. 21, no. 6, pp. 888–904, Jun. 2004.

[57] D. S. Zrnic and R. J. Doviak, "Velocity spectra of vortices scanned with a pulse-Doppler radar," *J. Appl. Meteorol. Climatol.*, vol. 14, no. 8, pp. 1531–1539, Dec. 1975.

[58] P. Kollias, B. A. Albrecht, and F. D. Marks, "Cloud radar observations of vertical drafts and microphysics in convective rain," *J. Geophys. Res., Atmos.*, vol. 108, no. D2, pp. 1–12, Jan. 2003.

[59] C. Unal, "Spectral polarimetric radar clutter suppression to enhance atmospheric echoes," *J. Atmos. Ocean. Technol.*, vol. 26, no. 9, pp. 1781–1797, Sep. 2009.

[60] A. Djafri, "Mapping of weather radar ground clutter using the digital elevation model (SRTM)," *Signal Image Process., Int. J.*, vol. 3, no. 4, pp. 135–151, Aug. 2012. [Online]. Available: http://www.aircconline.com/sipij/V3N4/3412sipij11.pdf

[61] M.-H. Golbon-Haghighi, G. Zhang, Y. Li, and R. Doviak, "Detection of ground clutter from weather radar using a dual-polarization and dual-scan method," *Atmosphere*, vol. 7, no. 6, p. 83, Jun. 2016. [Online]. Available: http://www.mdpi.com/2073-4433/7/6/83

[62] T. Liu and D. Li, "Convergence of the BFGS-SQP method for degenerate problems," *Numer. Funct. Anal. Optim.*, vol. 28, nos. 7–8, pp. 927–944, Aug. 2007.

[63] J. Hensman, N. Durrande, and A. Solin, "Variational Fourier features for Gaussian processes," *J. Mach. Learn. Res.*, vol. 18, no. 151, pp. 1–52, 2018.

[64] P. Stoica and Y. Selen, "Model-order selection: a review of information criterion rules," *IEEE Signal Process. Mag.*, vol. 21, no. 4, pp. 36–47, Jul. 2004.

[65] A. Roodaki, J. Bect, and G. Fleury, "Comments on 'joint Bayesian model selection and estimation of noisy sinusoids via reversible jump MCMC,'" *IEEE Trans. Signal Process.*, vol. 61, no. 14, pp. 3653–3655, Jul. 2013.

[66] S. E. Finder, E. Treister, and O. Freifeld, "Effective learning of a GMRF mixture model," *IEEE Access*, vol. 10, pp. 7289–7299, 2022.

[67] C. L. Matson and A. Haji, "Biased Cramér–Rao lower bound calculations for inequality-constrained estimators," *J. Opt. Soc. Amer. A, Opt. Image Sci.*, vol. 23, no. 11, pp. 2702–2713, 2006.

[68] M. Levin, "Power spectrum parameter estimation," *IEEE Trans. Inf. Theory*, vol. IT-11, no. 1, pp. 100–107, Jan. 1965.

[69] D. S. Zrnić, "Simulation of weatherlike Doppler spectra and signals," *J. Appl. Meteorol.*, vol. 14, no. 4, pp. 619–620, Jun. 1975.

[70] Mathworks. (2024). *Optimization Toolbox™ User's Guide R2024a*. [Online]. Available: https://www.mathworks.com

Tworit Dash (Graduate Student Member, IEEE) was born in Nayagarh, Odisha, India, in 1994. He received the B.Tech. degree from the Department of Instrumentation and Electronics Engineering, College of Engineering and Technology, Bhubaneswar, India, in 2016, and the M.Sc. degree (cum laude) in electrical engineering, telecommunication, and sensing systems track from the Delft University of Technology, Delft, The Netherlands, in 2020. He is currently pursuing the Ph.D. degree with the Microwave Sensing, Signals and Systems Group, Delft University of Technology, Delft, The Netherlands.

Hans Driessen received the M.Sc. and Ph.D. degrees from the Department of Electrical Engineering, TU Delft, Delft, The Netherlands, in 1987 and 1992, respectively.

Since then he has been employed with Thales Nederland BV, Hengelo, The Netherlands. He has held various positions as a System Designer of plot extraction and track processing, technical authority on tracking and data fusion; and Knowledge and Technology Manager in the area of algorithms for radar signal/data processing and radar management. He has been involved in the acquisition, execution and monitoring of a variety of (inter)national research projects, including EDA and EU FP6/7 Projects. He holds a partime position as an Associate Professor at the EEMCS Faculty, Microwave Signals Sensor and Systems Group, TU Delft, in the field of radar systems, waveforms, and processing.

O. A. Krasnov received the M.Sc. degree in radio physics from Voronezh State University, Voronezh, Russia, in 1982, and the Ph.D. degree in radio technique from the National Aerospace University "Kharkov Aviation Institute," Kharkiv, Ukraine, in 1994.

In 1999, he joined the International Research Center for Telecommunications and Radar (IRCTR), Delft University of Technology (TU Delft), Delft, The Netherlands. Since 2009, he has been a Senior Researcher at the Microwave Sensing, Signals and Systems (MS3) Section, Faculty of Electrical Engineering, Mathematics, and Computer Science (EEMCS), TU Delft, and became an Universitair Docent (Assistant Professor) there in 2012. His research interests include radar waveforms, signal and data processing algorithms for polarimetric radars and distributed radar systems, multi-sensor atmospheric remote sensing, optimal resource management of adaptive radar sensors, and distributed systems.

Dr. Krasnov has served as the Secretary for the 9th European Radar Conference (EuRAD-2012), Amsterdam, The Netherlands.

Alexander Yarovoy (Fellow, IEEE) received the Diploma degree (Hons.) in radiophysics and electronics and the Cand. Phys. Math. Sci. and Dr. Phys. Math. Sci. degrees in radiophysics from Kharkov State University, Kharkiv, Ukraine, in 1984, 1987, and 1994, respectively.

In 1987, he joined the Department of Radiophysics, Kharkov State University, Kharkiv, as a Researcher, where he became a Professor in 1997. From September 1994 to 1996, he was with the Technical University of Ilmenau, Ilmenau, Germany, as a Visiting Researcher. Since 1999, he has been with Delft University of Technology, Delft, The Netherlands. Since 2009, he leads there a Chair of Microwave Sensing, Systems and Signals. He has authored and co-authored more than 600 scientific or technical papers, eleven patents and fourteen book chapters. His main research interests are in high-resolution radar, microwave imaging and applied electromagnetics (in particular, UWB antennas).

Dr. Yarovoy has been member of numerous conference steering and technical program committees. He is the recipient of the European Microwave Week Radar Award for the paper that best advances the state-of-the-art in radar technology in 2001 (together with L. P. Ligthart and P. van Genderen) and in 2012 (together with T. Savelyev). In 2010, together with D. Caratelli, he got the best paper award of the Applied Computational Electromagnetic Society (ACES). In the period 2008-2017, he served as the Director of the European Microwave Association (EuMA). He served as the General TPC chair of the 2020 European Microwave Week (EuMW'20), as the Chair and TPC chair of the 5th European Radar Conference (EuRAD'08), as well as the Secretary of the 1st European Radar Conference (EuRAD'04). In 2023, together with Dr. I. Ullmann, N. Kruse, R. Gündel and Dr. F. Fioranelli he got the best paper award at IEEE Sensor Conference. He served also as the co-chair and TPC chair of the Xth International Conference on GPR (GPR2004). He has been serving on various editorial boards such as that of the IEEE TRANSACTION ON RADAR SYSTEMS. From 2011 to 2018, he served as an Associated Editor of the INTERNATIONAL JOURNAL OF MICROWAVE AND WIRELESS TECHNOLOGIES.